AD_____

AWARD NUMBER: W81XWH-10-2-0130

TITLE: Advanced Functional Nanomaterials for Biological Processes

PRINCIPAL INVESTIGATORS: Alexandru S. Biris, Ph.D.; Vladimir P. Zharov, Ph.D.

CONTRACTING ORGANIZATION: University of Arkansas at Little Rock

REPORT DATE: January 2014

TYPE OF REPORT: Final

PREPARED FOR: U.S. Army Medical Research and Materiel Command
Fort Detrick, Maryland 21702-5012

REPORT DOCUMENTATION PAGE

Form Approved
OMB No. 0704-0188

1. REPORT DATE	2. REPORT TYPE	3. DATES COVERED
01/15/2014	Final	24 Sept. 2010- 23 Oct. 2013

4. TITLE AND SUBTITLE

Advanced Functional Nanomaterials for Biological Processes

5a. CONTRACT NUMBER

5b. GRANT NUMBER
W81XWH-10-2-0130

5c. PROGRAM ELEMENT NUMBER

6. AUTHOR(S)
Alexandru S. Biris, Ph.D.

E-Mail: asbiris@ualr.edu

5d. PROJECT NUMBER

5e. TASK NUMBER

5f. WORK UNIT NUMBER

7. PERFORMING ORGANIZATION NAME(S) AND ADDRESS(ES)
University of Arkansas at Little Rock
2801 South University Avenue
Little Rock AR 72204-1099

8. PERFORMING ORGANIZATION REPORT

9. SPONSORING / MONITORING AGENCY NAME(S) AND ADDRESS(ES)

U.S. Army Medical Research and Materiel Command
Fort Detrick, Maryland 21702-5012

10. SPONSOR/MONITOR'S ACRONYM(S)

11. SPONSOR/MONITOR'S REPORT NUMBER(S)

12. DISTRIBUTION / AVAILABILITY STATEMENT
Approved for Public Release; Distribution Unlimited

13. SUPPLEMENTARY NOTES

14. ABSTRACT

During the course of this project, we performed research in the area of tissue engineering/bone regeneration and cancer nanotechnology. The primary focus of the tissue engineering program was to understand the biophysiological activity of the complex multicomponent nanopolymeric scaffolds in goat models for the regeneration of bone tissue and BMP delivery. For the cancer research, we focused on synthesizing highly functional nanomaterials that have both magnetic and spectroscopic properties. They were linked with targeting agents and used for successful Radio-Frequency (RF) driven thermal ablation of cancer cells *in vitro*. We also designed a platform technology for the accurate delivery of cancer cells in circulation based on a photothermal/photoacoustic approach.

15. SUBJECT TERMS: Tissue Engineering, Cancer detection, Cancer destruction, Nanoparticles

16. SECURITY CLASSIFICATION OF:			17. LIMITATION OF ABSTRACT	18. NUMBER OF PAGES	19a. NAME OF RESPONSIBLE PERSON
a. REPORT	b. ABSTRACT	c. THIS PAGE			USAMRMC
U	U	U	UU	41	19b. TELEPHONE NUMBER *(include area code)*

Table of Contents

Page

1. Introduction

The **Advanced Functional Nanomaterials for Biological Processes** research program integrated research conducted by investigators in several departments at the University of Arkansas at Little Rock (UALR)—the Center for Integrative Nanotechnology Sciences (CINS), Chemistry, and Applied Sciences—with that of physicians, faculty, and pathologists at the University of Arkansas for Medical Sciences (UAMS), the National Center for Toxicological Research (NCTR), and Kansas State University (KSU). This work encompassed outstanding research at the nanostructural level and the use of advanced multifunctional nanomaterials in biological applications with a focus on cellular biology. The primary goals were to understand the interaction between biological systems and nanomaterials, to study the potential toxicological effects of the nanomaterials, and to develop technologies that could later be extended to animal models for tissue engineering, targeted drug delivery, and cancer treatment. We developed and studied the following: A. Biodegradable Polymeric Nanocomposite Materials with Drug Delivery Capabilities for Tissue Engineering and Bone Regeneration; and B. Multifunctional Nanoparticles for Cancer Early Diagnosis, Specific Targeting, and Destruction.

2. Body

Part A: Tissue Engineering and Bone Regeneration

Aim 1. Optimize the composition of the prototype implant to determine the most effective polymeric matrix by in vitro studies

During the first year, we focused on the characterization and formulations of the composites. We worked on various concentrations of nano-hydroxyapatite (HA) concentrations in polyurethane films, and we established a correlation between the concentration of nano HA, the osteoblastic cellular proliferation, and the mechanical properties of the composites. The data were repeated for statistical analysis to be included in a peer-reviewed publication and a follow-up technical report. We also performed research at the interface of osteoblastic cells and nanostructural materials: We introduced various nanomaterials (carbon nanotubes, HA, TiO2, and silver nanoparticles) into the cellular media at various concentrations. We have found that the nanomaterials have the ability to significantly increase mineralization and affect gene expression of the cells.

We also developed a completely new material for tissue engineering/bone regeneration based on HA, gold nanoparticles, and graphene. We devised a one-step method in which Au and hydroxyapatite were used as a catalytic system in a chemical vapor deposition process and generated graphene structures at high temperatures with acetylene and methane as the carbon sources. Our *in vitro* studies have shown an extremely high level of biocompatibility.

Furthermore, in the first year of the project, we developed and studied a novel TiO2 nanotubular surface which, after plasma discharge treatment, provided a very strong cellular proliferation. In this work, we studied the biologically induced responses and the proliferation of mouse osteoblastic cells over TiO_2 nanotubular arrays synthesized by electrochemical anodization and subjected to surface plasma modification. The nanomorphology of the nanotubular structures closely mimics the surface topography of bone, a similarity which represents an important requirement for implant surface coatings. Moreover, the bone structure is known to be formed at nano- and micro-structural levels and with high porosity. The use of such nanostructures as the interface between the implant surfaces and the bone host tissue also has biological advantages

related to the continuous possible supply of fluid, ions, nutrients, proteins, and hormones through the gaps present between adjacent TiO_2 nanotubes. Moreover, the vertically aligned TiO_2 nanotubes display significantly larger surface areas than the flat Ti surfaces, contributing positively to the adherence and proliferation of osteoblastic cells. We demonstrated that the exposure of the nanotubular arrays to a plasma discharge treatment of various gases (O_2, N_2, O_2/N_2 combinations, and He) significantly enhanced cellular proliferation, as compared to the untreated TiO_2 nanotubular structures. The goal of this study was to prepare superior titania-based implant coatings by adjusting the structural morphology of the TiO_2 nano-tubular structures and introducing chemical modifications onto their surfaces.

The goal of this research project was to examine the effects of a novel nanoparticle polymeric composite matrix on neovascularization, early bone formation in a critical bone defect, and antibiotic delivery as studied in a caprine model of bone trauma. We hypothesized that this novel composite of nanoparticles, bioabsorbable polymers, and hydroxyapatite would stimulate early neovascularization and rapid bone healing. Our long-term goal is to develop an optimized composite to be used as a drug delivery vehicle for treatment of compromised tissues in the face of infection. If successful, this program will become the basis for several platform technologies that can be used for bone regeneration and drug delivery. The process will make use of scaffolds built with bio-degradable/biocompatible polymeric materials and nano- and micro-materials for enhanced cellular activity.

We have performed research at the interface of osteoblastic cells and nanostructural materials such as graphitic nanostructures and studied their impact on cellular minearalization and gene activity. As a result, we have optimized the composition of the prototype implant to determine the most effective polymeric matrix by *in vitro* studies. Aim 1 has therefore been completed. In the second year of the project, however, we continued to pursue new materials for bone tissue regeneration. We demonstrated the effects of tubular, carboxylated MWCNTs, and carboxylated nano- and micro-sized Gn sheets on bone cell mineralization as two dissimilar morphologies.[1-7]

Aim 2. Adjust the implant configuration for antibiotic delivery effectiveness

AIM 2. ADJUST THE IMPLANT CONFIGURATION TO PROVIDE THE MOST EFFECTIVE ANTIBIOTIC DELIVERY SYSTEM.

We did perform mechanical studies of polymer composites with various concentrations of HA. We identified the fact that the wt.% of HA in the polymeric film, changes drastically their mechanical properties. Once these films were incorporated into 3D scaffolds, drug elution studies have been performed.

Aim 3. Test implantable polymeric scaffolds with and without antibiotics on goat models (KSU)

We first developed a strategy for the *in vivo* goat model studies. Dr. David Anderson, leader of the effort to be conducted at Kansas State University, visited UALR for two days during which extensive discussions concerning the research approach were conducted.

The goal of this research aim was to examine the effect of a novel nanoparticle polymeric composite matrix on neovascularization and early bone formation in a critical bone defect, with and without bacteria present, as studied in a caprine model of bone trauma.

We hypothesized that this novel composite of nanoparticles, bioabsorbable polymers, and hydroxyapatite will stimulate early neovascularization and rapid bone healing. The long-term goal is to develop an optimized composite such that this could be used as a drug delivery vehicle for treatment of compromised tissues in the face of infection.

All *in vivo* procedures were completed in the second year of the project. The study protocol required 48 goats (12 per treatment group). A total of 53 goats were used. (Five goats were replaced early in the study because of medical illness such as pneumonia, anesthetic death, and orthopedic implant failure.)

We then began to analyze and compile data for physical examination, radiographic, DEXA, and HD thermography data. Serum and interstitial fluid samples for antibiotic and BMP-2 analysis were submitted to the laboratory and designated for completion in December of 2012. Bones for biomechanical testing were harvested and submitted to the MTS testing laboratory. These tests were scheduled to be conducted in November of 2012 to be completed by December 2012. Bone defect specimens were submitted to the histology laboratory and were scheduled to be completed by January of 2013. Histomorphology studies were to be completed by March of 2013.

High definition thermal imaging of the medial aspect of the tibia (mid-diaphyseal ostectomy site) was conducted for goats from day +1 to day +55. Surface thermography is an indication of vascular perfusion and inflammation.

Figure 1 shows an increase in surface temperature at the surgical site during the first 2 weeks after implantation in those goats having matrix + antibiotics +/- BMP-2, only.

This was followed by a return to baseline by day 14 and a lower surface temperature throughout the remainder of the study.

The increased temperature noted for control and BMP-2 goats during days 21-45 corresponds to the increased bone proliferation during this period.

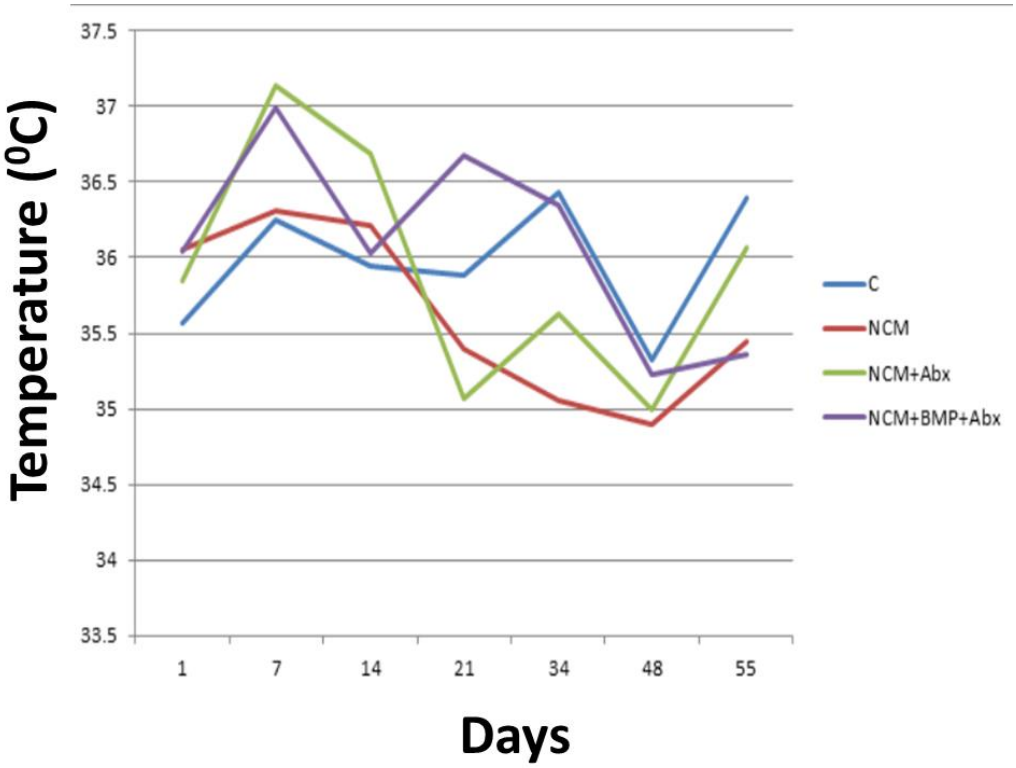

Figure 1. High definition thermal imaging of the medial aspect of the tibia (mid-diaphyseal ostectomy site) for goats from day +1 to day +55. (C-Control, NCM-nanostructuralmatrix, NCM+ABX – matrix and antibiotics, NCM+ABX+BMP – matrix and antibiotics and BMP).

Projected timeline for study completion:

Sample / Data	Acquisition end date (Date of last tissue or serum harvest)	Analysis end date (Date of completion of testing – actual or projected)	Completion Date
Radiographs	August 17, 2012	August 17, 2012	October 2012
DEXA	August 17, 2012	August 17, 2012	October 2012
Serum analysis	August 17, 2012	December 2012	January 2013
Interstitial fluid analysis	August 17, 2012	December 2012	January 2013
HD Thermography	August 17, 2012	August 17, 2012	October 2012
Tissue biopsy	July 20, 2012	October 2012	November 2012
Biomechanical testing	August 17, 2012	November 2012	December 2012
Histomorphometry	August 17, 2012	January 2013	March 2013

Based on projected times for completion of sample processing, testing, and analysis, we expected to complete the project within six (6) months.

The long-term goal of this research is to develop an optimized composite such that this could be used as a drug delivery vehicle for treatment of compromised tissues in the face of infection. We

would expect 50% more bone formation in the same period of time, or 50% more rapid bone formation as benchmarks for performance.

Thermographic imaging revealed a transient increase in skin surface temperature at the implantation site during the first 7 days after surgery for the goats receiving the antibiotic and antibiotic-BMP impregnated matrices. Skin surface temperature was similar throughout the remainder of the study period.

Radiographic scoring (Figure 2): Cranial-to-caudal radiographic images were scored using a 1 to 5 scale (1 = no bone reaction; 2 = focal bone formation; 3 = multifocal bone formation; 4 = proliferative bone response; 5 = bone bridging bone defect. The nanoparticle matrix stimulated early bone formation in all groups as compared to controls. Matrices without drug plateaued and were similar to controls at day 60. Nanoparticle matrices containing rhBMP-2 induced multifocal bone formation within 14 days, proliferative response within 30 days, and proliferative to bridging bone by 60 days after creation of the defect. (BMP group > Control, $p < 0.01$; BMP group > Matrix, $p < 0.01$). The biomechanical testing results for the tibias of the goats after implantation is shown in Figure 3 and 4.

Figure 2. Radiographic scoring of the bone formation kinetics for the animal studies in various conditions.

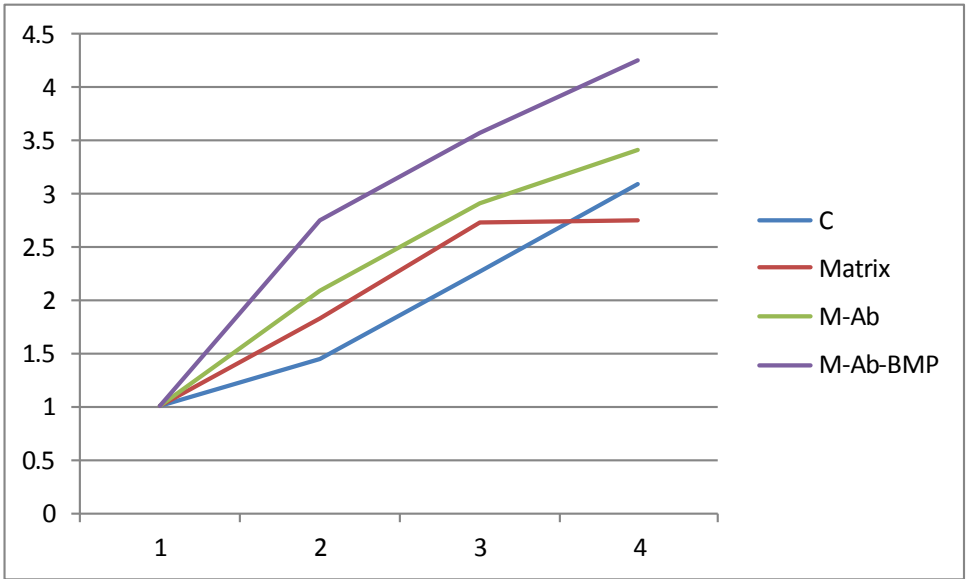

Figure 3. Biomechanical testing: Three point bending tests were performed on tibias harvested at day 60 after surgical implantation. Any tibia for which the defect had insufficient integrity to allow testing was assigned a test result of "0".

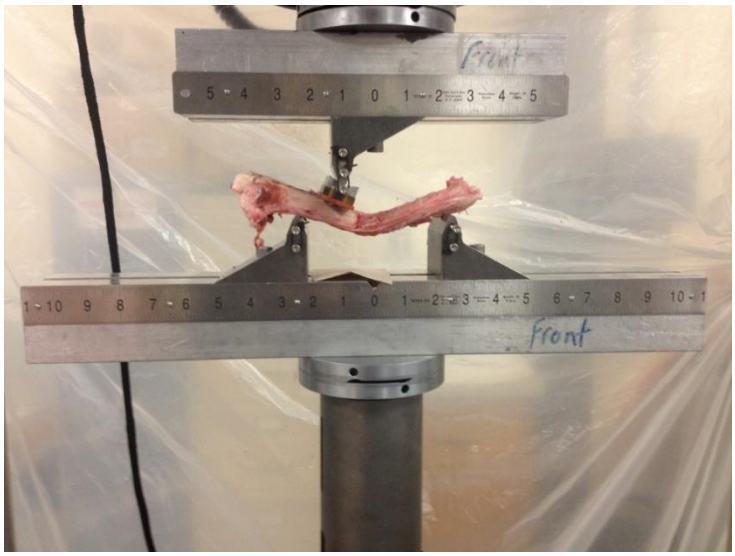

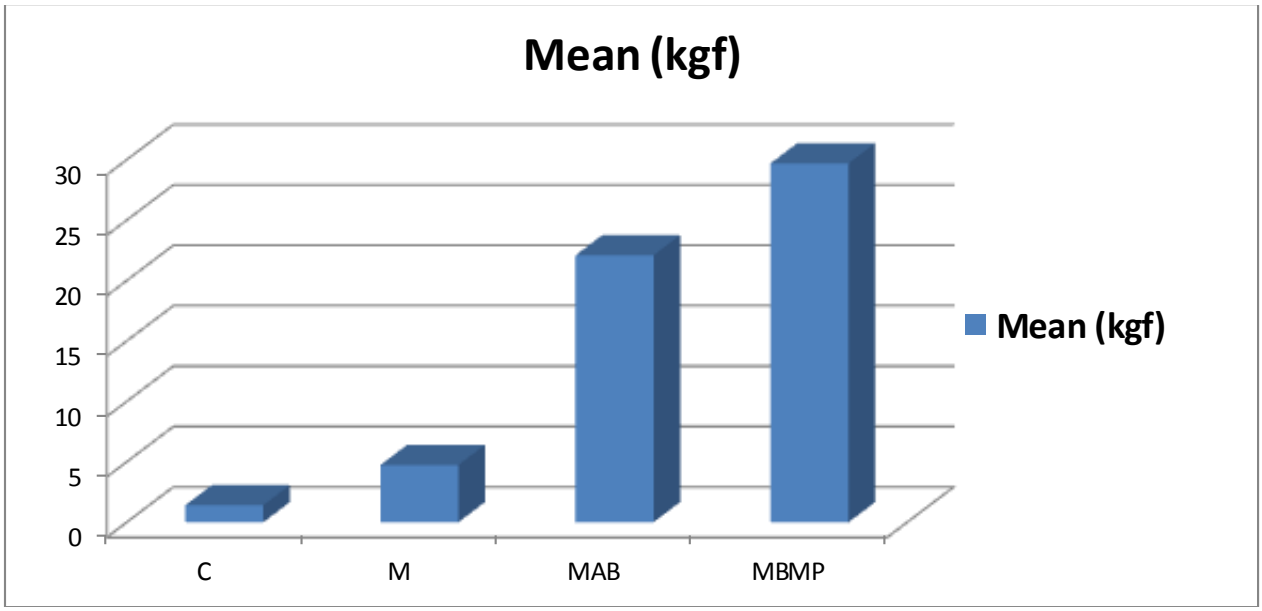

Goats having matrices impregnated with antimicrobial drugs or with rhBMP-2 in addition to antimicrobial drugs had markedly greater resistance to bending as compared with control goats and goats in which matrix alone was implanted. The mode of failure for control goats was lack of tissue integrity. This contrasts with rhBMP-2 goat in which all specimens failed by fracture at the bone-implant interface.

Histomorphometry: All study tibias were harvested and histomorphometry slides made from undecalcified specimens. Sections were cut in the frontal plane so as to include the entire defect as well as bone proximal and distal to the defect. Bone on-growth and in-growth within the defect or implant were assessed using light microscopy and fluorence at 450 nm (calcein

fluorescent bone label). Bone formation was significantly increased in all goats having matrix implants. Matrices impregnated with rh-BMP-2 had markedly greater bone formation than other treatment group goats (Figure 4-6).

Figure 4. Example Control Goat: Histomorphometry of control goat defects done 60 days after surgery revealed little new bone formation as evidenced by lack of new bone mineralization fronts.

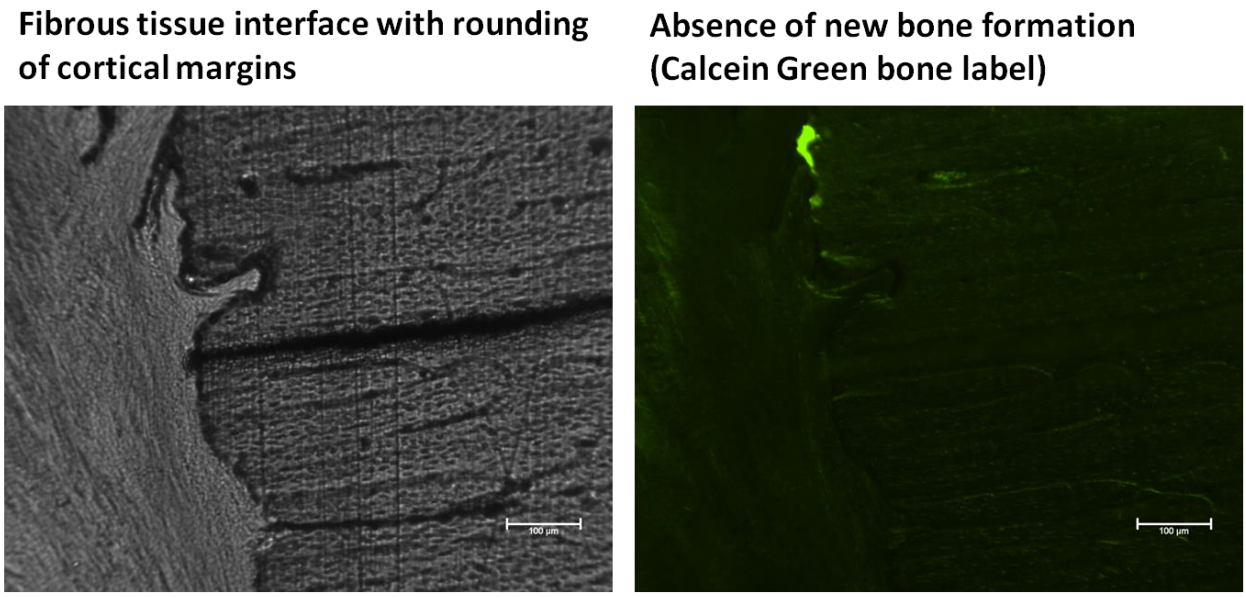

Figure 5. Example Antimicrobial impregnated Matrix Goat: Bone on-growth and in-growth was apparent in histomorphometry sections from goats having antimicrobial impregnated matrix.

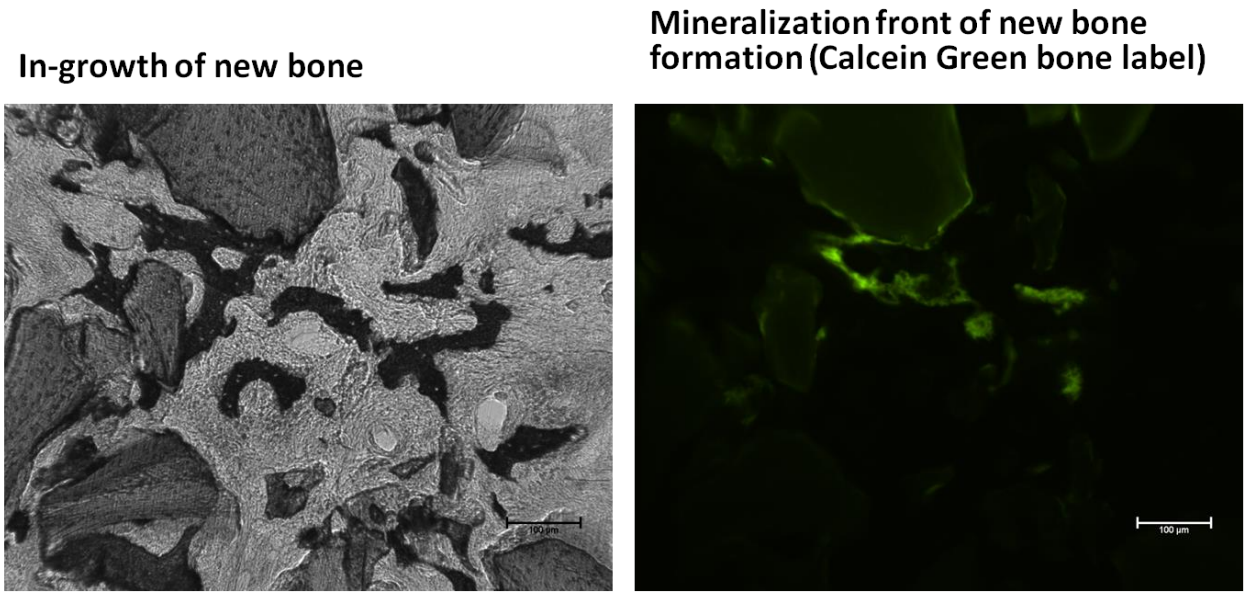

Figure 6. Example antimicrobial and rh-BMP-2 impregnated matrix goat.

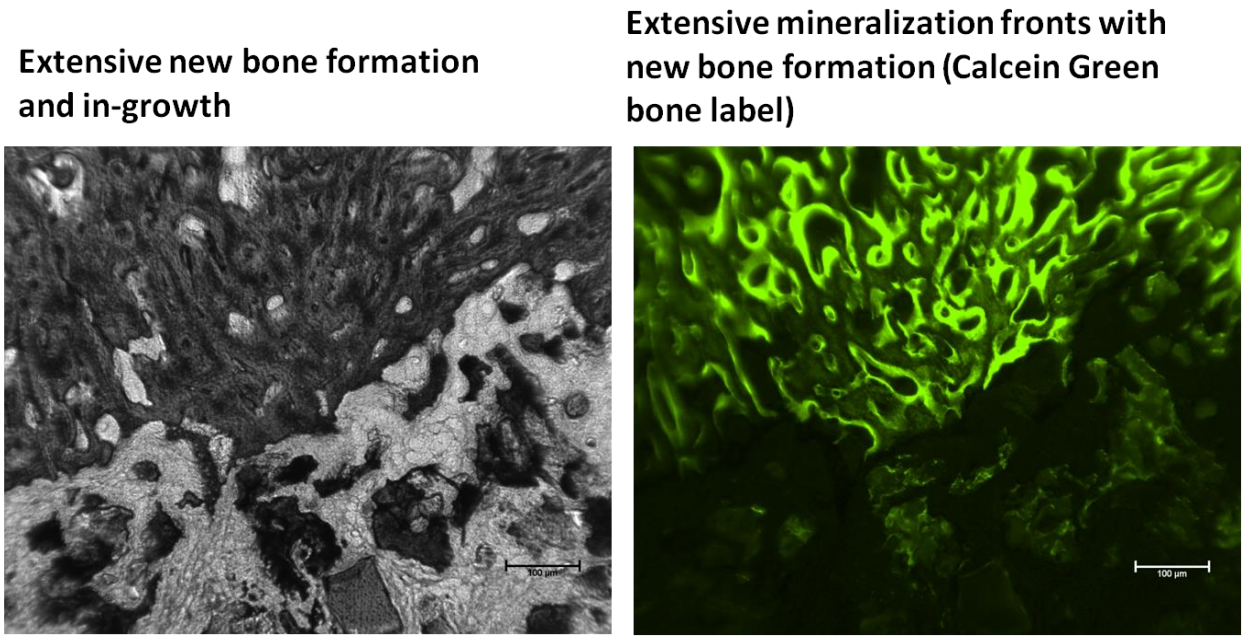

Discussion: The results of this study showed that this nanoparticle composite matrix has tremendous potential for bone tissue engineering applications. Although bone tissue response to the matrix, alone, was modest, the drug delivery application resulted in substantial new bone formation. This response was clearly evident on histomorphometry but was most remarkable during biomechanical testing. The lattice work of new bone formed within the matrix and spanning the defect provided clinically relevant resistance to bending force.

The nanocomposite material developed for this study was designed to be biocompatible, easily handled by the surgeon, provide for incursion of bodily fluids and development of a network of blood vessels into the device to allow access to the responding cells via porosity, provide space while the bone is being formed, and to be resorbed over time leaving replacement bone tissue. This study showed that the nanoparticle matrix was biocompatible, stimulated rapid bone healing through in-growth and on-growth of new bone, provided a scaffold for formation of a strong lattice work of new bone, and had excellent surgeon handeling.

Part B: Cancer Early Diagnosis, Specific Targeting, and Destruction

Aim 1. Synthesis of nanomaterials with low toxicity that can absorb electromagnetic radiation

a. Synthesis of multifunctional nanomaterials for thermal ablation
b. Cytotoxic studies of various magnetic nanomaterials (UALR and NCTR)

During the first year of the project, we developed and studied nanomaterials with tunable magnetic properties and high bio-compatibility. We had previously used these nanomaterials for radio-frequency driven thermal ablation of cancer cells *in vitro*. By linking the magnetic

nanomaterials to growth factors (EGF), we proved an enhanced cellular killing rate *in vitro*. The results were best for a breast model cancer cell line (MCF7).

The current study focused on designing EGF-conjugated C/Fe nanoparticles to be used for the specific ablation of human pancreatic cancer cells (Panc-1) and breast cancer cells (MCF-7) *in vitro*. The physical properties of the C/Fe MNPs are presented along with their comparative efficiency to kill the cancer cells alone or when bioconjugated with EGF molecules. The two cancer cell lines appeared to present different sensitivity levels to the RF-induced localized heating, with the Panc-1 showing a much higher resistance compared to the MCF-7 cell lines to the RF induced heat into the C/Fe MNPs. This system is presented as a potential model for the development of highly specific cancer treatment technologies that involve targeting agents, magnetic nanomaterials and low frequency RF excitation for the inducement of localized heat into the cells. We also created magnetic nanoparticles with a variety of metal cores (Co, Fe, and Fe/Co), as reported in our publication in the *International Journal of Nanomedicine*. (See Appendix A.)

We continued the research in the area of toxicology in collaboration with Dr. Syed Ali (NCTR/FDA) and showed that the surface chemistry of graphitic nanomaterials (carbon nanotubes) plays a primary role in the induced toxicity and genotoxicity. This work was published in *ACS Nano*.[8-13]

Multifunctional Magnetic Nanoparticles for Synergistic Enhancement of Cancer Treatment by Combinatorial Radio Frequency Thermolysis and Drug Delivery

Here, we reported that multimodal, graphitic carbon-coated iron (C/Fe) magnetic nanoparticles can be employed in two ways with synergistic efficiency. On one hand, magnetic nanoparticles can function as carriers by means of an easy drug-loading mechanism (π-π stacking); on the other, they can absorb energy from a radio-frequency (RF) source and thus generate local heat inside cancer cells. Controlled drug release from the loaded particles can be triggered by RF-induced temperature or by decreased pH levels (typical in the neoplastic cellular environments). At the same time, RF treatment can synergistically enhance the therapeutic efficacy of drugs. Two types of drugs were used as models in this work: Doxorubicin (Adriamycin), a universal model for cancer chemotherapy for more than 50 years, and Erlotinib (Tarceva), the first biological drug designed to treat pancreatic cancer, having been approved by the FDA in 2006. we developed multimodal, magnetic C/Fe MNPs used as drug nanocarriers, as well as thermal agents under RF-excitation. The PEG functionalization of the 7-10 nm magnetic nanoparticles made them stable in biological systems while showing low toxicity. Two drugs, Doxorubicin (DOX) and Erlotinib, were successfully loaded onto the MNP surface through π-stacking. The loading capacity, release, and reduction level of the drug cytotoxicity were found to depend on the drugs themselves. Drug release rates, especially for DOX, were enhanced 4.8 times when exposed to the RF excitation. The temperature increases in the magnetic nanoparticles triggered by radio-frequency treatment combined with the anticancer drug therapy, acted supra-synergistically. The DOX efficiency was enhanced to the high level of a 3.5 fold increase in cellular death. Such complex approaches to cancer treatment could work synergistically in inducing cellular death and decreasing chemoresistance to cytostatic drugs. Also, the combination therapy could result in the use of lower drug concentrations, reducing the overall occurrence of adverse effects, and yet achieving improved tumor control.

The manuscript was published in *Advanced HelathCare Materials*, 2012. (See Appendix A.)

Single-walled carbon nanotubes as specific targeting and Raman spectroscopic agents for detection and discrimination of single human breast cancer cell

In this research effort, covalent Epcam-SWCNT complexes were developed and proposed as high-sensitivity Raman nano-agents for the detection and discrimination of cancer cells from normal cells. The prepared nano-agents were able to detect single cancer cells from among thousands of normal cells within 30 minutes of the targeting process. The targeting/detection complex was prepared by mixing anti-Epcam antibody with surface-functionalized SWCNTs and was characterized by using a transmission electron microscope (TEM) and Raman spectroscopy.

Iron oxide nanoparticle-based radio-frequency thermotherapy for human breast adenocarcinoma cancer cells

In the third year of the project, iron oxide nanoparticles (IONPs) with diameters of 15, 25, and 41 nm were evaluated as mediators of thermal cytotoxicity under radio-frequency (RF) exposure. The 25 nm IONPs were found to be the most efficient of the three in killing cancer cells at 350 kHz low-frequency RF irradiation. However, at a higher frequency of 13.56 MHz, 15 nm IONPs produced the highest percentage of cell death. Moreover, the killing effect was concentration-dependent in that a higher concentration of IONPs resulted in increased cellular death. Size-dependent internalization of IONPs in MCF-7 cells was quantified by using inductively coupled-plasma mass spectrometry (ICP-MS). Dark-field microscopy and transmission electron microscopy (TEM) revealed that MCF-7 cells internalize IONPs through endocytosis after 24 hours of incubation. In addition, after RF treatment, the cancer cells underwent the apoptosis process, and the level of reactive oxygen species (ROS) increased significantly after hyperthermia. Scanning electron microscopy (SEM) and TEM further established that the ultrastructure morphological changes in the cancer cells originated from the apoptosis process.

Our research demonstrated that IONPs are excellent candidates for the hyperthermia treatment of human breast cancer cells. Nanoparticle size and RF frequency are critical parameters that influence the optimum level of the hyperthermia effect. For 350 kHz lower frequency RF, the 25 nm IONPs proved to be the most efficient in killing the cancer cells. At a higher frequency (13.56 MHz) of RF, smaller sized (15 nm) IONPs are the most effective. RF-induced heat treatment was found to damage the cells' plasma membrane and mitochondria membrane, thus greatly increasing ROS levels and causing cellular apoptosis.

The manuscript was published in *Biomaterials Science*. (See Appendix A.)

Calcium Channel Blocking and Nanoparticles-Based Drug Delivery for Treatment of Drug-Resistant Human Cancers

Cancer cell chemoresistance is one of the most serious limitations to successful cancer treatment and one of the factors that is responsible for the possible recurrence of the disease. Here, we combined a calcium channel blocker, Verapamil, with an alternative method of delivering the anti-cancer drug, doxorubicin, using nanostructural materials to reduce the cellular resistance to chemotherapeutics agents. The effect of this complex approach on cellular viability was investigated using various assays in both a time- and concentration-dependent manner: WST-1, flow cytometry cell viability assay, fluorescence microscopy, DNA fragmentation, and TUNEL labeling of apoptotic cells. All of these analytical assays confirmed the ability to reduce the chemoresistance of the cancer cells based on the proposed procedure.

Aim 2. In vivo magnetic enrichment and photoacoustic detection of circulating tumor cells (Dr. Zharov-UAMS)

Based on our preliminary studies and ongoing research in Zharov's Phillips Classic Laser and Nanomedicine Laboratories at the University of Arkansas for Medical Sciences (UAMS), during the first year of this project, we completed the development of a multifunctional multimodal nanotechnology-based platform of *in vivo* flow cytometry using support from this specific project, as well as additional resources. This platform utilizes the ability of the photoacoustic (PA) method to detect circulating tumor cells (CTCs) directly in the blood stream with possibility for their photothermal (PT) ablation. This platform opens the door also to use Raman-based detection methods allowing either label-free detection of CTCs with distinctive intrinsic properties (e.g., strong pigmentation or Raman-related scattering) or using low-toxicity strongly absorbing nanoparticles (NPs) as PT, PA, and Raman contrast agents. In these particular projects, we added a well-established fluorescent technique to verify PA/PT data in animal models. With these multimodal platforms, we have demonstrated for the first time nonlinear PA flow cytometry (PAFC) for real-time monitoring of the clearance rate of various NPs.

***Experimental Setup*.** Upgrades were made to the multifunctional setup resulting in a 4-color *in vivo* PAFC platform by the integration of 4 high-pulse repetition lasers with the following parameters (wavelength, pulse width, pulse rate, pulse energy): 1) 532 nm, 25 ns, 30 kHz, 40 µJ; model: LUCE 532, Bright Solutions, Italy; 2) 671 nm, 24 ns, 1-50 kHz; 40 µJ; model: QL671-500, CrystaLaser; 3) 820 nm, 8 ns, 10 kHz, 78 µJ; model: LUCE 820-10kHz, Bright Solutions, Italy; and 4) 1064 nm, 10 ns, 500 kHz, 100 µJ; model: MOPA-M-10, MultiWave Photonics, Portugal. We also developed hardware and software for the time-color coding of PA signals by introducing time delays between laser pulses with different wavelengths, using a universal digital delay/pulse generator (DG645, Stanford Research Systems) for triggering each laser. As a result, using the time-resolved PA mode, we were able to detect, simultaneously, four PA signals corresponding to four different wavelengths (532/671/820/1064 nm) from the same fast flowing single circulating tumor cells (CTCs). We incorporated a continuous wave (CW) diode laser 488 nm, 45 mW (Power technology, Little Rock, AR), for simultaneous PA and fluorescent detection of CTCs (with fluorescent labels or genetically engineered with green fluorescent protein [GFP]), and cells labeled with magnetic and gold NPs conjugated with antibodies (Abs) and other biomolecules to specific CTC markers. In the *in vitro* study, we used a PT microscope that was developed previously. This multifunctional setup was built on the technical platform of an invert Olympus IX81 microscope-spectrometer (420-2500 nm) with fluorescent and PT thermolens modules. We added optics for the delivery of radiation from 7 lasers (4 with high pulse rate, optical parametric oscillator [OPO], diode, and PT probe). We added a focused cylindrical transducer (20–50 MHz; focal length, 4–10 mm; Panametrics) to detect CTCs located in relatively deep tissue including bones. To make the nano-platform more universal, we have explored various NPs, including the carbon nanotubes (CNTs), golden carbon nanotubes (GNTs), magnetic NPs (MNPs), and gold nanorods (GNRs), with tunable plasmonic resonances in the spectral range of 520 nm-1100 nm.

Experimental results. Using an upgraded laser system, we performed detailed studies of the PA spectra of normal mouse blood vessels. In particular, we discovered that, in addition to the widely used "window tissue transparency" (650 nm-950 nm), the spectral range of 1030-1100 nm is also attractive for PAFC, because of the comparable low background absorption, availability of both lasers with high pulse repetition rates, and NPs with strong absorption (e.g., GNTs or GNRs). Non-conjugated NPs along with NPs conjugated with Abs to cancer cell receptors (e.g., folate, EpCam, and CD24) and also to leukocytes (CD45, to exclude nonspecific binding) were intravenously (i.v.) injected into the tail veins of anesthetized animals

in different concentrations followed by the monitoring of blood vessels using selected lasers. (See selected data in Figure 7.)

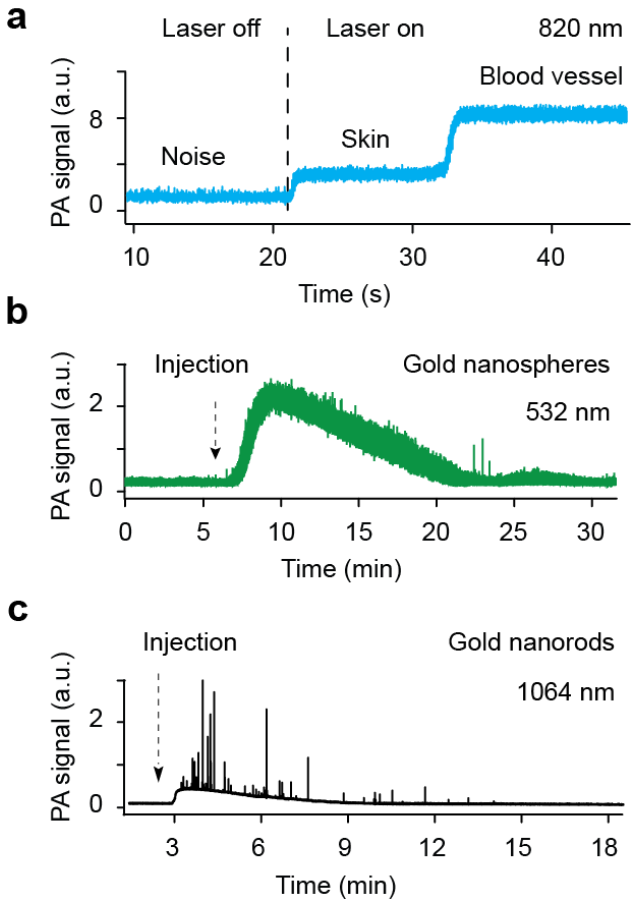

Figure 7. PA monitoring of NP clearance rates. (**a**) *In vivo* PA signal levels from mouse ear vein and surrounding skin, compared to baseline noise, when the laser is off. Laser parameters: wavelength, 820 nm; fluence, 0.2 J/cm^2; pulse rate, 10 kHz. (**b**) PA monitoring of the clearance rate of gold nanoparticles in mouse ear vessel. Laser parameters: 532 nm, 0.4 J/cm^2, 9 kHz. (**c**) PA monitoring of hybrid magnetic–gold nanorod NPs in mouse ear vessel. Laser parameters: 1064 nm, 0.5 J/cm^2, 9 kHz.

We determined that NPs in concentrations less than 1×10^9 GNRs and 3×10^8 GNTs per mouse did not produce detectable PA signals above the blood background. We also found that most NPs produced a short term (few minutes) increased background, as a result of the transient presence of the many NPs and, especially, their difficult to control small rare aggregates in the detected volume immediately after the injection. This background elevation quickly disappeared due to redistribution of NPs in the whole body. The selected cancer cells (e.g., MDA-MB- 231 and others) were labeled priory (i.e., *in vitro*) by bioconjugated NPs. The bioconjugation efficiency (around 86-95%) was verified by fluorescent imaging using additional fluorescent tags and by PT cytometry (Aim1). Then these cells were introduced i.v. into the mice in a concentration range of 10^4-10^6/mL to mimic targeting of CTCs. PAFC demonstrated the ability to count and identify these cells using specific PA-spectral signatures at different laser wavelengths. To explore whether cancer cells can be selectively targeted *in vivo*, we applied an

i.v. injection of cancer cells followed by a second injection of NPs (e.g., GNRs) at a concentration of 10^9 per mouse, bioconjugated with Abs (EpCam, folate, CD24) to label the CTCs. Fifteen minutes after injections (i.e., when small NP aggregates were already cleared), the PAFC of the mouse ear vessels demonstrated the strong, rare PA signals associated with labeled CTCs. To exclude possible nonspecific binding of NPs with leukocytes, we injected NPs (at 820 nm) bioconjugated with Abs to CD45 receptors of leukocytes.

We also developed *in vivo* PA bone flow cytometry (Figure 8a) for real-time detection of circulating normal cells (e.g., stem or immune), abnormal cells (e.g., CTCs), and NPs in bones. We used fiber delivery laser radiation for noninvasive irradiation skin above mouse tibia near the site where blood vessels enter into bone. Intravenous injection of CNTs (2 mg/ml, 50 µl solution) in mouse circulation led to appearance of PA signal traces (Figure 8b). Compared to monitoring CNTs in ear and abdominal blood vessels in bone, PA signals were more rare with lower amplitude and required increased laser energy (300-500 mJ/cm^2). Scanning of laser beam along the bone revealed rare stationary PA signals associated with the accumulated CNTs. Similar results were obtained for cancer cells targeted by GNRs. We believe that after further optimization this technology has a potential for early diagnosis of bone metastasis (noninvasive bone marrow biopsy), cancer recurrence, and detection of NPs in bone tissue.

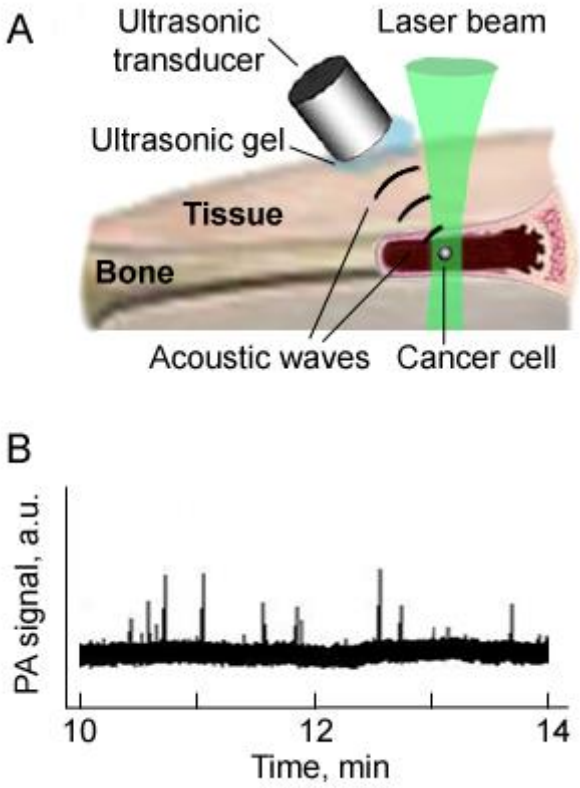

Figure 8. *In vivo* PA bone flow cytometry. (A) Schematics. (B) Noninvasive *in vivo* detection of circulating CNTs in mouse tibia.

We found that spectral specificity of multicolor PAFC and multiplex PT nanotherapy may be limited by the relatively broad absorption bands of PT/PA contrast agents (80 to 300 nm for plasmonic NPs. To overcome this problem, we proposed nonlinear PT and PA spectroscopy as follows: If the laser wavelength is away from the absorption centers and the laser-induced

temperature is slightly below the threshold for nonlinear effects (e.g., bubble formation), linear signals are generated; however, a shift of the laser wavelength toward the absorption centers leads to an increase in energy absorption and hence in the temperature of the absorbing zone. A temperature slightly above the evaporation threshold induces sudden nanobubble formation accompanied by nonlinear signal amplification. As a result, spectrally dependent signal amplification will lead to the sharpening of PT/PA resonances near the centers of the absorption peaks. To provide sharpening of the absorption dip, laser energy must be close to the threshold in the center of the dip. This will lead to spectrally dependent signal amplification if the laser wavelength shifts away from the dip's center accompanied by an increase in absorbed energy and hence more profound bubble formation. In a preliminary study, new nonlinear spectroscopy demonstrated ultrasharp resonances up to a few nanometers (4-10 nm) wide in broad plasmonic spectra of gold-based NPs, in particular GNRs and GNTs. It is important that nonlinear ultrasharp PT/PA spectral resonances are accompanied by amplification of PT/PA effects that may lead to dramatic increases in both the specificity and sensitivity of PAFC diagnosis and the efficiency of PT nanotherapy.

According to these findings, the advanced *in vivo* multicolor PAFC platform with the high pulse repetition rate lasers was developed, and its utility was demonstrated for the detection of NPs and mimic CTCs targeted by conjugated NPs in blood vessels and bone tissue. If successful, this technology would have tremendous clinical utility in terms of identifying metastatic diseases at an early stage, instituting therapeutic targeting of CTCs before they become a clinical problem, and monitoring response to treatment. A robust, low-cost, portable medical device that delivers fiber-based laser radiation that is safe for humans could be developed for routine daily use. The discovered ultrasharp PA–plasmonic resonances may provide further progress in multicolor PAFC of multiple cancer markers.

During the second year of this project, we continued upgrading the experimental setup. In particular, we installed a new high-speed card and developed a second generation of software to improve the collection of photoacoustic (PA) signals using, simultaneously, several high-pulse rate lasers with different wavelengths. Using this hard and software, we measured the dependence of PA signal amplitudes on laser pulse rate for different samples include mouse blood and tumor cells. We found that the maximum signal-to-noise ratio can be obtained with a pulse rate in the range of 10-500 kHz. In addition, after theoretical modeling and testing of different nanoparticles (NPs) and tumor cells, we determined that the optimal laser pulse duration for effective generation of PA signals from circulating tumor cells (CTCs) labeled by gold or magnetic NPs should be around 1 ns, whereas our current laboratory lasers provide only 10 ns. This leads to a decrease in the PA flow cytometry (PAFC) sensitivity of more than 10 times. To avoid this problem, we placed an order for a customized laser with the required parameters; however, this laser was not delivered until August of 2012, which led to some delay in the experimental studies.

We purchased a new customized Ytterbium fiber laser (model YLP-R-0.3-A1-60-18, IPG Photonics) with the following parameters: wavelength, 1060 nm; pulse duration range, 0.8, 5 and 10 ns; pulse repetition rate, 10kHz-500kHz; pulse energy, 20 uJ-300 uJ. All technical parameters such as frequency, pulse energy, average power, energy fluence, pulse width, and energy stability (2-5% during 10 minutes) were tested. Next, we built a PAFC setup with the aforementioned laser and delivery laser radiation using optic fibers with optical tips consisting of combination spherical and cylindrical lenses. The focal length of the optical tips was in the range of 3-8 mm with a linear laser beam shape of 70 µm x 1 mm. To detect PA signals, we have purchased high-frequency focused ultrasound transducers: 1) spherical, model V317 (Panometric (Olympus); central frequency, 20 MHz, lateral resolution 150 µm; 2) customized spherical (lateral resolution 40 µm, frequency 32 MHz; 3) customized spherical (lateral

resolution 70 µm, frequency 18 MHz); 4) customized cylindrical (lateral resolution 40 µm, frequency 32 MHz); and 5) customized cylindrical (lateral resolution 70 µm, frequency 18 MHz).

The parameters of the PAFC were tested *in vitro* with different samples including filtered black beads (0.19 µm, 0.76 µm, and 6 µm), filtered carbon nanotubes (200 nm), filtered magnetic nanoparticles (50 nm); selected cancer cells, mouse blood, and other absorbing samples. As a result, we have determined that the PAFC with Ytterbium fiber laser provides relatively stable photoacoustic (PA) signals with level instability of 5-10% in our conditions of measurement. The signal-to-noise ratio for the same sample was as follows: 42 for V317; 120 for spherical; and 165 for cylindrical. We developed different combinations of fiber tips and ultrasound transducers. To optimize schemes, we used two XYZ-stages (Thorlabs, Inc.): one for fixation of the fiber tip and another for fixation of ultrasound transducers. Their different spatial position and orientation (space angle) were tested to find the best position for tip and transducer. As a result, we determined the optimal spatial configuration of fiber tip and transducer. We have also purchased a computer, model Precision T3500 Workstation (Dell Inc.), together with a high-speed analog-to-digit card (see above) ATS9350, 12 bit, 500 MS/s digitizer with 128 MB dual-port memory (Alazar Technologies Inc.), which was installed into the computer. Our computer engineer developed customized software, which takes PA data in real time mode and transfers them to a computer database. After saving the data, this software provides analyses of PA signal trace, peak-to-peak maximum, signal-to-noise ratio, standard deviation, etc.

The PAFC prototype was used for the detection of CTCs *in vitro* in vessel phantoms based on Minipump variable flow device (Fisher Scientific) with different inner tube diameters in a range of 800 µm-2mm and flow velocity of 5-30 mm/s. Using data obtained and electronic, optical, and mechanical components (e.g., customized cart, power supplies, electrical filters, trigger, keyboard and monitor holder, cooling system, wires and cables, electrical shielding, switchers, buttons, etc.) purchased with other financial support, we built a clinically relevant PAFC prototype (Figure 9). Laser, transducer, preamplifier, and all other mentioned components were mounted inside the cart. Using the optimized optical parts, we installed and tested the final optic scheme which included different lenses, mirrors, photodetector, power and energy meter, LED-red pilot beam, six levels wheel filter, safety shutter, and optic fiber (most from Thorlabs, Inc.). Finally, *in vitro* and *in vivo* on animal model, we determined the optimal laser pulse repetition rate (10-50 kHz) for detection of cancer cells directly in the bloodstream using an energy fluence of 28-35 mJ/cm ^{2}.

Figure 9. Experimental clinically relevant PAFC prototype.

The described hard and software also allowed us to detect simultaneously PA and fluorescent signals from CTCs. (Previously, we monitored these signals separately.) It provided a unique platform for verification of new PA data with well-established fluorescent technique. In addition to the linear laser beam configuration, we also developed a galvanometer-mirror-based system providing linear fast (0.5 ms) scanning of focused circular laser beams across vessels. This system provides more sensitive detection of CTCs due to the reduction of background signals from blood. We also tested the capability of magnetic nanoparticles (MNPs) conjugated to folate to target selectively tumor cells compared to normal blood cells. Then we verified the feasibility of magnetically capturing tumor cells labeled by MNPs *in vitro.*

Using this advanced setup, we continued an evaluation of the PAFC's diagnostic value *in vivo* using a tumor-bearing nude mouse model. Specifically, we tested molecule targeting and detection of CTCs on tumor-bearing mouse models using multicolor (four wavelengths) *in vivo* PAFC. In addition, we performed a study of the magnetic capture of flowing CTCs labeled by magnetic NPs (MNPs) followed by PA detection of captured CTCs. We found that the use of MNPs offers the advantage of the magnetic capture of cells. However, the near-infrared (NIR) contrast of MNPs was much lower (10-30-fold) compared to gold NPs, in particular gold nanorods (GNRs). Taking into account the linear PA signal enhancement we had previously discovered using gold NPs, we evaluated the nonlinear PA properties of MNPs with silica layer (siMNPs). At low laser energy (*i.e.,* in linear mode), siMNPs demonstrated 1.8 to 2.5-fold increased PA signals compared to MNPs without silica layer. At higher laser energy, we observed a 20- to 35-fold nonlinear PA signal amplification, a phenomenon named by us as a giant PA amplification. This can be explained by the favorable thermal acoustic and bubble-related properties of siMNPs for the generation of nonlinear PA effects including silica-induced rigid restriction for thermal expansion of the heated magnetic core. We also observed the amplified PA spectra within the NIR window tissue transparency due to more profound bubble-associated nonlinear effects at higher MNP absorption. In addition, the magnet-induced clustering of siMNPs provided a nonlinear PA signal increase due to the enhanced nanobubble formation around strongly-absorbing siMNP clusters. These data suggest that magnetic-induced clustering of MNPs within individual cells can yield enhancement of PA signals accompanied by nanobubble formation around the overheated local zone with increased absorption. Finally, using new siMNPs conjugated with folate, we confirmed the capability of these NPs to target selectively tumor cells. In addition, the PAFC demonstrated 10-fold enhanced sensitivity compared to conventional MNPs.

As described in the first-year report, we determined that, even after significant attention of laser radiation in the bone tissue, the laser energy is still enough to generate readable PA signals from strongly absorbing objects inside bones using focused ultrasound transducers. In particular, intravenous injection of carbon nanotubes (CNTs) led to the appearance of PA signal traces from the mice's tibia. Similar results were obtained during the second year for breast cancer cells (MDA-MD-321-GFP) targeted by GNRs with a maximum absorption at 670 nm. The GNRs conjugated with folate were intravenously injected in the tumor-bearing mouse model at week 4 after tumor inoculation. We observed rare PA signals from the tibia irradiated by a high-pulse-rate laser (10 kHz) at 671 nm (Figure 10). These signals were associated with individually targeted CTCs. PA scanning cytometry revealed also rare stationary PA signals associated with the captured in bone CTCs. This technique, after further optimization, has the potential for early and painless diagnosis of bone cancer metastasis (noninvasive bone marrow biopsy) through

the administration of strongly absorbing NPs functionalized to identify specific cancer cells markers. The identification of targeted cells was performed as follows. Healthy bones produce low-level background PA signals because low concentrations of NPs are randomly and nonspecifically distributed in the bone tissue as compared to a high local concentration of NPs that is found in cells causing bone metastasis.

The goal of this work was to develop a clinically relevant PAFC setup for the ultrasensitive, noninvasive detection of CTCs using the principle of PAFC. We designed and built a laser-based PAFC with 1064 nm laser, fiber delivery of laser radiation, and a small ultrasound transducer attached to the skin. We tested the main parameters of the prototype *in vitro* on phantom and in animal mode. The expected outcome—the assessment of a patient's entire blood volume (in adults ~5 L)—will provide a significant (100-1000-fold) enhancement to the sensitivity of CTC detection using PAFC as compared to the existing assays. If pilot clinical trials in the future are successful, this technology could represent a breakthrough in the early detection and treatment of cancer metastasis.

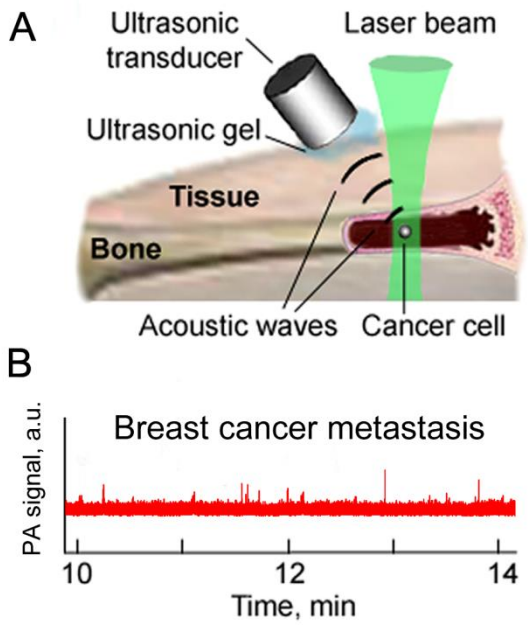

Figure 10. *In vivo* PA bone flow cytometry. (A) Schematics. (B) Noninvasive *in vivo* molecular targeted detection of CTCs in mouse tibia.

During the final year of the project, we continued to test the experimental setup using a customized Ytterbium fiber laser (model YLP-R-0.3-A1-60-18, IPG Photonics; wavelength, 1060 nm; pulse duration range, 0.8-10 ns; pulse repetition rate, 10 kHz-500 kHz; pulse energy, up to 300 µJ) *in vivo* on animal model. We focused on the safety of this device for potential use in humans, in particular, cancer patients. The PAFC device was previously evaluated using laser settings below the maximum permissible exposure (MPE) for skin as defined by the American National Standard for Safe Use of Lasers Z136.1-2007 (e.g., energy fluence ≤100mJ/cm^2 for 1060-1064 nm laser operating at 10 Hz and lower fluences as the pulse rate increases; or average power ≤1W/cm^2 for 1060-1064 nm laser light exposures greater than 10s). Previous clinical trials, employing similar PA diagnostic devices, demonstrated the safety of these laser parameters. These studies included the assessment of blood vessels and the

properties of the blood, such as hemoglobin and oxygenation, in vessels of the hand and neck. However, since the sensitivity of our PAFC device is proportional to the laser fluence and the number of nanoparticles per one cell, it became necessary to exceed the mentioned MPE. Laser output was adjusted to provide adequate sensitivity to ensure detection of circulating tumor cells (CTCs) and minimize false negative results (missing some CTCs) while being limited to a level to avoid side effects. For example, we currently tested laser fluence at 5.2J/cm^2 for pulse rate of 10 kHz at linear laser beam shape (6.5 x 800 µm). Because we observed overheating effects on mouse skin, including burning within a small laser beam area (red spot up to 1 mm in size), we provided additional modeling laser-induced photothermal effects in biotissue and confimed our previous hypothesis that burning effects can be excluded by decreasing the laser pulse repetition rate from 10 kHz to 1 kHz. However, the available laser does not provide a pulse rate of 1 kHz. Our previous results using electro-mechanical schematics did not allow us to obtain stable laser energy at 1 kHz and a chopper produced electromagnetic artifacts. During the last three months of the third year of the project, we developed new schematics using a new chopper and triggering system. The testing on animal model (mice) demonstrated that we could use a laser fluence of 5 -10 J/cm^2 without skin burning.

In addition to safety issues, clinical applications of *in vivo* photoacoustic (PA) flow cytometry (PAFC) for detection of CTCs in deep blood vessels can be hindered by laser light scattering, resulting in a PAFC sensitivity and resolution loss. To partially solve this problem, we explored rapid optical clearing (OC) procedure. On animal model, OC effect was achieved in 10-20 min by sequent skin cleaning, microdermabrasion, and glycerol application enhanced by massage and sonophoresis. Using mouse 0.83 mm skin layer covering glass capillary with mouse blood (simple *in vitro* phantom of blood vessels), we demonstrated a 1.6-fold decrease in laser spot blurring accompanied by a 1.6-fold increase in PA signal amplitude from blood. Thus, without increasing the laser energy, we were able to increase PA sensitivity1.5-2 fold by reducing light scattering in biotissue.[14-21]

Aim 3. Study of the anti-cancer activity of carbon nanotubes modified with phenolic acids

Ovarian cancer cell line (OVCAR-3) was purchased from American Type Culture Collection (ATCC, Manassas, VA, USA) and maintained in RMPI-1640 medium supplemented by 20 % fetal bovine serum (FBS), 0.1 % insulin, and 100 U/ml penicillin, and 100 U/ml streptomycin at 37 ˚C under 5% CO2. The cells were primarily cultured in 75cm2 tissue culture flasks and incubated until confluent. The cells were then sub-cultured by 0.25% trypsin-EDTA (Gibco BRL, Rockville, MD, USA).

WST-1 cytotoxicity assay

Mitochondrial metabolic activity and cell death were studied using WST-1 colorimetric detection kit (Roche). Briefly, OVCAR-3 cells were plated in 96-well plates at a density of 50×10^4 cells /well with 100µl of growth medium. After 24h, the cells were supplemented with the desired concentrations of single-walled carbon nanotubes (SW) (20, 40 µg/ml) and CPE conjugated SW (SWCPE) (20, 40 µg/ml) and the CPE alone as a control (20, 40 µg/ml). Normal growth medium was used as a negative control. The WST-1 assay was performed at 3 time points (24, 48, and 72 h following treatment). 10 µl of WST-1 reagent was added to all samples and incubated for 2-4 h at 37 ºC. The absorbance of each sample at 450 nm was assessed with the iMark microplate reader (BIO-RAD, USA). The means were collected from three independent experiments and 6 samples for each condition.

Results

To evaluate the cytotoxicity of CPE, SW, and SWCPE, WST-1 assay was employed, which is a reliable method to assess the cells' metabolic activity and cell death. As shown in Figure 11 below, there was no significant effect on the mitochondrial metabolic activity even after 72hrs. The optical density values were almost the same for all conditions as compared with control samples. Unfortunately, the acticvity of CPE was not found to increase in the presence of nanoparticles. More studies are planned.

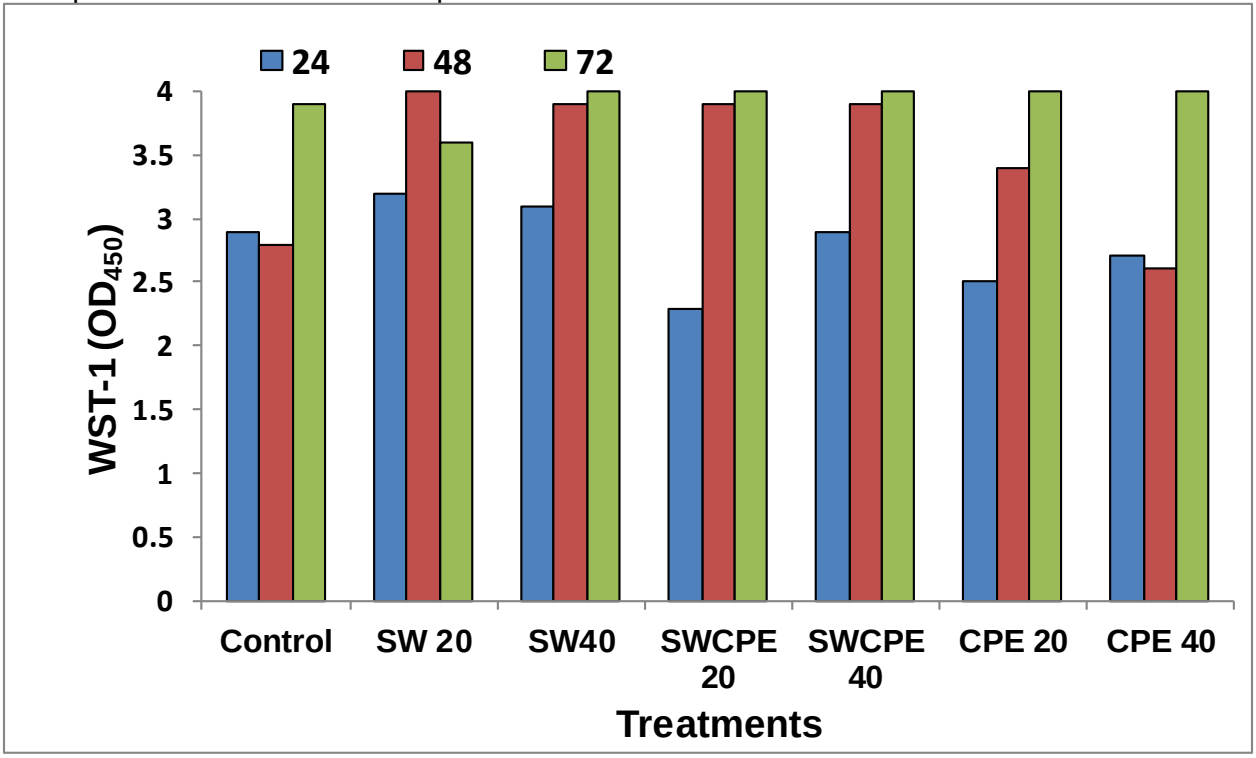

Figure 11. WST-1 based cytotoxicity assay results. OVCAR-3 cells were incubated for 24, 48, and 72 h with free SW, CPE, and SWCPE complexes using 2 different concentrations (20 and 40µg/ml). The data are presented as the mean of the optical density collected from 3 independent experiments and (n=6) for each.

3. Key Research Accomplishments

- We began the study of multifunctional nanocomposites for bone regeneration. We linked their mechanical, structural and compositional properties with their mechanical and bio-compatibility properties and published the research results in one journal article. A second article was begun.
- We successfully synthesized magnetic nanomaterials (with cores of Fe, Co or Fe/Co) and 2-4 layers of graphitic carbon for radio-frequency driven thermolysis. The *in vitro* tests showed the high ability of such nanomaterials to induce heat under a RF excitation.
- We linked the magnetic nanomaterials to EGF as a specific targeting molecule, and we proved enhanced cellular destruction.
- We proved that nanomaterials can induce greater mineralization in bone cells and upregulate genes related to bone formation. We hypothesized that such a study could result in a possible vaccine for osteoporosis.

- We successfully studied the cytotoxic properties of a large number of nanomaterials *in vitro.*
- We developed a platform technology for using photo-thermal/photo-acoustic techniques for the accurate detection of cancer cells/nanomaterials in circulation.
- We showed that graphitic materials can increase the osteogenesis of bone cells.
- We finished the *in vivo* studies for bone regeneration (goat models) and began conducting the data analysis.
- We successfully synthesized magnetic nanomaterials (with cores of Fe, Co, or Fe/Co) and 2-4 layers of graphitic carbon for radio-frequency driven thermolysis. The *in vitro* tests showed a high ability of such nanomaterials to induce heat under RF excitation. In the second year of the project, we also used these nanomaterials for drug delivery with excellent results.
- We linked the magnetic nanomaterials to EPCAM as a specific targeting molecule, and we demonstrated excellent specificity in cell targeting and Raman detection.
- We continued to study the cytotoxic properties of a large number of nanomaterials *in vitro.*
- We continued to refine the platform technology for using photo-thermal/photo-acoustic techniques for the accurate detection of cancer cells/nanomaterials in circulation.

4. Reportable Outcomes

1.Y. Zhang, Y. Xu, Z. Li, T. Chen, S. M. Lantz, P.C. Howard, M. G. Paule, *et al.* Mechanistic Toxicity Evaluation of Pristine and PEGylated Single-Walled Carbon Nanotubes in Neuronal PC12 Cells. *ACS Nano*. **5**, 7020-33, (2011).

2. A. Karmakar, M. W. Mahmood, A. Ghosh, T. Mocan, C. Iancu, L. Mocan, D. Todea Iancu, A. Fejleh, P. Fejleh, Y.Xu, *et al*. Raman Spectroscopy as a Detection and Analysis Tool for In Vitro Specific Targeting of Pancreatic Cancer Cells by EGF-Conjugated Single-Walled Carbon Nanotubes. *Journal of Applied Toxicology*. **32**, 365-375, (2012).

3. A. R. Biris, M. Mahmood, L.D. Mihaela, E. Dervishi, F. Watanabe, *et al.* Novel multicomponent and biocompatible nanocomposite materials based on few-layer graphenes synthesized on a gold/hydroxyapatite catalytic system with applications in bone regeneration. *Journal of Physical Chemistry C*. **115**, 18967-76, (2011).

4. A. Biswas, H. Zhao, T. Wang, T. C. Ovaert, C. Slaboch, *et al*. Mineral Concentration Dependent Modulation of Mechanical Properties of Bone-Inspired Bionanocomposite Scaffold. *Applied Physics Letters*. **99**, 013702-5, (2011).

5. M. Mahmood, Y. Xu, D. Casciano, A.S. Biris. Engineered nanostructural materials for application in cancer biology and medicine. *Journal of Applied Toxicology*. **32**, 10-19, (2012).

6. A. Karmakar, Y. Xu, M.W. Mahmood, A. Fejleh, Y. Zhang, *et al.* Radio-Frequency induced *in vitro* thermal ablation of cancer cells by EGF functionalized multimodal graphitic coated magnetic nanoparticles. *Journal of Materials Chemistry*. **23**, 12761-9, (2011).

7. A.R. Biris, S. Simon, D. Lupu, I. Misan, C. Iancu, *et al.* Near infrared optical absorption and corresponding thermal properties of single- and double-walled carbon nanotubes as correlated with their Raman scattering properties. *Carbon*. **49**, 4403-11, (2011).

8. A. Orza, O. Soritau, A. Florea, L. Olenic, D. Rus Ciuca, *et al*. Electrically Conductive Gold Coated Collagen Nanostructures for Enhanced Placental-derived Mesenchymal Stem Cells Differentiation and Proliferation. *ACS Nano*. **5**, 4490–503, (2011).

9. M. Mahmood, Z. Li, D. Casciano, M. V. Khodakovskaya, T. Chen, *et al*. Nanostructural materials increase mineralization in bone cells and affect gene expression through miRNA regulation. *Journal of Cellular and Molecular Medicine.* **15**, 2297-2306, (2011).

10. M. Mahmood, P. Fejleh, A. Karmakar, A. Fejleh, Y. Xu, *et al.* Enhanced Bone Cells Growth and Proliferation on TiO2 Nanotubular Substrates Treated by RF Plasma Discharge. *Advanced Engineering Materials.* Special Issue: 3D-Imaging of Materials and Systems. **13**, B95–B101, (2011).

11. Y. Xu, M. Mahmood, A. S. Biris. Multifunctional Nanomaterials for Bio-medical Applications: The onset of Nanomedicine. Wiley Book chapter, (2011).

12. A. Karmakar, S. Bratton, E. Dervishi, A. Ghosh, M. Mahmood, *et al*. Ethylenediamine Functionalized-Single Walled Nanotube (f-SWNT)-Assisted In Vitro Delivery of Oncogene Suppressor p53 Gene to Breast Cancer MCF-7 Cells. *International Journal of Nanomedicine*. **6**, 1045–55, (2011).

13. A. Biswas, I. S. Bayer, H. Zhao, T. Wang, F. Watanabe and A. S. Biris. Design and Synthesis of Biomimetic Multicomponent All-Bone-Minerals Bionanocomposites. *Biomacromolecules*. **1**, 2545–9, (2010).

14. Y. Zhang, S. Ali, E. Dervishi, Y. Xu, Z. Li, *et al.* Cytotoxicity Effects of Graphene and Single-Wall Carbon Nanotubes in Neural Phaeochromocytoma-Derived PC12 Cells, *ACS Nano*. **4**, 3181–6, (2010).

15. A. de la Zerda, K. Jin-Woo, E.I. Galanzha, S.S. Gambhir, V.P. Zharov. Advanced contrast nanoagents for photoacoustic molecular imaging, cytometry, blood test and phototohermal theranostics. *Contrast Media and Molecular Imaging journal.* **6**, 346-369, (2011).

16. V.P.Zharov. Ultrasharp nonlinear photothermal and photoacoustic resonances and holes beyond the spectral limit. *Nature Photonics*. **5**, 110-6, (2011).

17. M. Sarimollaoglu, D.A. Nedosekin, Y. Simanovsky, E.I. Galanzha, V.P. Zharov. In vivo photoacoustic time-of-flight velocity measurement of single cells and nanoparticles. *Optics Letters*. **36**, 4086-8, (2011).

18. D.A. Nedosekin, M. Sarimollaoglu, E.I Galanzha, R. Sawant, V.P. Torchilin, V.V. Verkhusha, J. Ma, M.H. Frank, A.S. Biris, V.P. Zharov. Synergy of of photoacoustic and fluorescence flow cytometry circulating cells with negative and positive contrasts. *Journal of Biophotonics.* **6**, 425-434, (2013).

19. D. Nedosekin, M. Sarimollaoglu, Y. Ye, E.I. Galanzha, V.P. Zharov. In vivo ultra-fast photoacoustic flow cytometry of circulating human melanoma cells using near-infrared high-pulse rate laser. *Cytometry*. **79A**, 825-33, (2011).

20. V.V. Tuchin, A. Tarnok, V.P. Zharov. In vivo flow cytometry: A horizon of opportunities. *Cytometry A.* **79A**, 737-45, (2011).

21. E.I. Galanzha, M. Sarimollaoglu, D.A. Nedosekin, S.G. Keyrouz, J.L. Mehta, V.P. Zharov. In vivo flow cytometry of circulating clots using negative photototherma l and photoacoustic contrasts. *Cytometry*. **79A**, 814-24, (2011).

22. E.I. Galanzha, V.P.Zharov. In vivo photoacoustic and phototohermal cytometry for monitoring multiple blood rheology parameters. *Cytometry*. **79A**, 746-57, (2011).

23. M. Proskurnin, E.I. Galanzha, D.M. Mock, V.P. Zharov. In vivo multispectral photoacoustic and photothermal flow cytometry with multicolor dyes: A potential for real-time assessment of circulation, dye-cell interaction, and blood volume. *Cytometry*. **79A**, 834-47, (2011).

24.Y. Xu, A. Karmakar, W. E. Heberlein, A. R. Biris, and A. S. Biris. Multifunctional Magnetic Nanoparticles for Synergistic Enhancement of Cancer Treatment by Combinatorial Radio Frequency Thermolysis and Drug Delivery. *Advanced Healthcare Materials*. **1**, 493-501, (2012).

25. M. Mahmood, Y. Xu, D. Casciano, A. S. Biris. Nanomaterials for Bio-medical Applications: A Review. *Journal of Applied Toxicology*. **32**, 10-19, (2012).

26. T. Mustafa, F. Watanabe, W. Monroe, M. Mahmood, Y. Xu, L. Saeed, A. Karmakar, D. Casciano, S. Ali, A. S. Biris. Electron Microscopic Analysis of Cellular Uptake of Gold Nanoparticles by MC3T3-E1 Mouse Osteoblast Cells. *Journal of Nanomedicine and Nanotechnology*. **2**,1-7, (2011).

27. A. Karmakar, M. W. Mahmood, A. Ghosh, T. Mocan, C. Iancu, L. Mocan, D. T. Iancu, A. Fejleh, P. Fejleh, Y. Xu, E. Dervishi, S. L. Collom, Z. Li, A. R. Biris, M. Khodakovskaya, D. Casciano, A. S. Biris. Raman Spectroscopy as a Detection and Analysis Tool for In Vitro Specific Targeting of Pancreatic Cancer Cells by EGF-Conjugated Single-Walled Carbon Nanotubes. *Journal of Applied Toxicology*. **32**, 365-375, (2012).

28. Y. Xu, W. E. Heberlein, M. Mahmood, I. A. Orza, A. Karmakar, A. R. Biris, D. Casciano, A. S. Biris. Progress in Materials for Thermal Ablation of Cancer Cells. Featured Paper, *Journal of Materials Chemistry*, 22, 20128-20142, (2012).

29. D.A. Nedosekin, M. Sarimollaoglu, E.I. Galanzha, R. Sawant, V.P. Torchilin, V.V. Verkhusha, J. Ma, M.H. Frank, A.S. Biris, V.P. Zharov. Synergy of photoacoustic and fluorescence flow cytometry of circulating cells with negative and positive contrasts. *J Biophotonics* 6, 425-434, (2012).

30. E.I. Galanzha, V.P. Zharov. Photoacoustic flow cytometry. *Methods*. **57**, 280-96. (2012).

31. J. Shao, R.J. Griffin, E.I. Galanzha, J.W. Kim, N. Koonce, J. Webber, T. Mustafa, A.S. Biris, D.A. Nedosekin, V.P. Zharov. Photothermal nanodrugs: potential of TNF-gold nanospheres for cancer theranostics. *Sci Rep*. **3**, 1293, (2013).

32. D.A. Nedosekin, M. Sarimollaoglu, E.I. Galanzha, R. Sawant, V.P. Torchilin, V.V. Verkhusha, J. Ma, M.H. Frank, A.S. Biris, V.P. Zharov VP. Synergy of photoacoustic and fluorescence flow cytometry of circulating cells with negative and positive contrasts. *J Biophotonics*. **6**, 425-34, (2013).

33. M.A. Juratli, M. Sarimollaoglu, E. Siegel, D.A. Nedosekin, E. Galanzha, J.Y. Suen, V.P. Zharov. Real-time monitoring of circulating tumor cell release during tumor manipulation using in vivo photoacoustic and fluorescent flow cytometry. *Head Neck*. 2013 Aug 3. doi: 10.1002/hed.23439. [Epub ahead of print].

5. Conclusion

During the course of the project, we developed a very aggressive research program resulting in numerous publications in peer-reviewed journals concerning our tissue-engineering/bone regeneration and cancer studies. Multifunctional polymeric nanocomposite materials were synthesized, and their mechanical properties, as well as their bio-compatibility (cellular proliferation), were studied. As a result of the research program in tissue engineering, we proved the ability to regenerate bone tissue in a very controlled manner and reduced time. All our studies performed with goat models indicated bone formation in as early as 14 days. The platform technology proved to be extremely reliable for the regeneration of large bone gaps of around 2-3 cm. We would like to further expand the research to larger bone defects with complex morphologies and shapes. This work has proved to have a major potential for battlefield-type injuries resulting in bone loss. For cancer research, we developed several platform technologies for cancer targeting and treatment. A photothermal/photoacoustic approach was developed with the successful outcome of detecting cancer cells in circulation. We also developed multifunctional magnetic nanoparticles that were linked with targeting molecules for the specific targeting of cancer cells *in vitro*. The nanomaterials proved to be bio-compatible with a low level of toxicity and, under RF radiation, generated a high enough level of heat to kill the cells. In partnership with the National Center for Toxicological Research (NCTR)/FDA, we studied the cyto- and genotoxicity of a few classes of nanomaterials and proved that the shape, size, and chemical surface properties of the nanomaterials are very important factors in their cytotoxicity. Future studies will be designed to further improve the technology.

6. References

1. Y. Zhang, Y. Xu, Z. Li, T. Chen, S. M. Lantz, P. C. Howard, M. G. Paule, W. Slikker Jr., F. Watanabe, T. Mustafa, A. S. Biris, S.F. Ali. Mechanistic Toxicity Evaluation of Pristine and PEGylated Single-Walled Carbon Nanotubes in Neuronal PC12 Cells. *ACS Nano*. **5**, 7020-33, (2011).

2. A. R. Biris, M. Mahmood, L. D. Mihaela, E. Dervishi, F. Watanabe, T. Mustafa, B. Grigore, B. Mihaela, B. Simion, A. S. Biris. Novel multicomponent and biocompatible nanocomposite materials based on few-layer graphenes synthesized on a gold/hydroxyapatite catalytic system with applications in bone regeneration. *Journal of Physical Chemistry C*. **115**, 18967-76, (2011).

3. A. Biswas, H. Zhao, T. Wang, T. C. Ovaert, C. Slaboch, I. S. Bayer, A. S. Biris. Mineral Concentration Dependent Modulation of Mechanical Properties of Bone-Inspired Bionanocomposite Scaffold. *Applied Physics Letters*. **99**, 013702-013705, (2011).

4. A. Orza, O. Soritau, A. Florea, L. Olenic, D.R. Ciuca, C. Mihu, M. Diudea, D. Casciano, A. S. Biris. Electrically Conductive Gold Coated Collagen Nanostructures for Enhanced Placental-derived Mesenchymal Stem Cells Differentiation and Proliferation. *ACS Nano*. **5**, 4490–4503, (2011).

5. M. Mahmood, Z. Li, D. Casciano, M. V Khodakovskaya, T. Chen, A. Karmakar, E. Dervishi, Y. Xu, T. Mustafa, F. Watanabe, A. Fejleh, M. Whitlow, M. Al-Adami, A. Ghosh, A. S. Biris.

Nanostructural Materials Increase Mineralization in Bone Cells and Affect Gene Expression Through miRNA Regulation. *Journal of Cellular and Molecular Medicine*, **15**, 2297-2306 (2011).

6. M. Mahmood, P. Fejleh, A. Karmakar, A. Fejleh, Y. Xu, G. Kannarpady, H. Ishihara, R. Sharma, Z. Li, A. Ghosh, S. Trigwell, F. D. Hardcastle, D. Casciano, A. S. Biris. Enhanced Bone Cells Growth and Proliferation on TiO_2 Nanotubular Substrates Treated by RF Plasma Discharge. *Advanced Engineering Materials*, Special Issue: 3D-Imaging of Materials and Systems. **13**, B95–B101, (2011).

7. A. Biswas, I. S. Bayer, H. Zhao, T. Wang, F. Watanabe, A. S. Biris. Design and Synthesis of Biomimetic Multicomponent All-Bone-Minerals Bionanocomposites. *Biomacromolecules*, **1**, 2545–2549, (2010).

8. A. Karmakar, M. W. Mahmood, A. Ghosh, T. Mocan, C. Iancu, L. Mocan, D.T. Iancu, A. Fejleh, P. Fejleh, Y. Xu, E. Dervishi, S. L. Collom, Z. Li, A. R. Biris, M. Khodakovskaya, D. Casciano, A.S. Biris. Raman Spectroscopy as a Detection and Analysis Tool for In Vitro Specific Targeting of Pancreatic Cancer Cells by EGF-Conjugated Single-Walled Carbon Nanotubes. *Journal of Applied Toxicology*, **32**, 365-375 (2012).

9. A. Karmakar, Y. Xu, M. W. Mahmood, A. Fejleh, Y. Zhang, L. M. Saeed, T. Mustafa, S. Ali, A. R. Biris, A. S. Biris. Radio-Frequency induced *in vitro* thermal ablation of cancer cells by EGF functionalized multimodal graphitic coated magnetic nanoparticles. *Journal of Materials Chemistry*, **23**, 12761-9, (2011).

10. A. R. Biris, S. Simon, D. Lupu, I. Misan, C. Iancu, D.T. Iancu, I.R. Ilie, E. Dervishi, Y. Xu, A. Biswas, A. S. Biris. Studies on near infrared optical absorption and corresponding thermal properties of single- and double-walled carbon nanotubes as correlated with their Raman scattering properties. *Carbon*, **49**, 4403-4411(2011).

11. A. Karmakar, S. Bratton, E. Dervishi, A. Ghosh, M. Mahmood, Y. Xu, L.M. Saeed, T. Mustafa, D. Casciano, A. Pandya-Radominska, A. S. Biris. Ethylenediamine Functionalized-Single Walled Nanotube (f-SWNT)-Assisted In Vitro Delivery of Oncogene Suppressor p53 Gene to Breast Cancer MCF-7 Cells. *International Journal of Nanomedicine*, **6**, 1045–1055, (2011).

12. Y. Zhang, S. Ali, E. Dervishi, Y. Xu, Z. Li, D. Casciano, A. S. Biris. Cytotoxicity Effects of Graphene and Single-Wall Carbon Nanotubes in Neural Phaeochromocytoma-Derived PC12 Cells. *ACS Nano*, **4**, 3181–3186, (2010).

13. A. de la Zerda, J.W. Kim, E.I. Galanzha, S.S. Gambhir, V.P. Zharov. Advanced contrast nanoagents for photoacoustic molecular imaging, cytometry, blood test and phototohermal theranostics. Wiley's *Contrast Media and Molecular Imaging*. **6**, 346-369, (2011).

14. V.P. Zharov. Ultrasharp nonlinear photothermal and photoacoustic resonances and holes beyond the spectral limit. *Nature Photonics*. **5**, 110-116 (2011).

15. M. Sarimollaoglu, D.A. Nedosekin, Y. Simanovsky, E.I. Galanzha EI, V.P. Zharov. In vivo photoacoustic time-of-flight velocity measurement of single cells and nanoparticles. *Optics Letters*. **36**, 4086-4088 (2011).

16. D.A. Nedosekin, M. Sarimollaoglu, E.I. Galanzha, R. Sawant, V.P. torchilin, V.V. Verkhusha, J. Ma, M.H. Frank, A.S. Biris, V.P. Zharov. Synergy of photoacoustic and fluorescence flow cytometry circulating cells with negative and positive contrasts. *Journal of Biophotonics*. **6**, 425-434 (2013).

17. D. Nedosekin, M. Sarimollaoglu, J.-H. Ye, E.I. Galanzha, V.P. Zharov. In vivo ultra-fast photoacoustic flow cytometry of circulating human melanoma cells using near-infrared high-pulse rate laser. *Cytometry*. **79A**, 825-833 (2011).

18. V.V. Tuchin, A. Tarnok , V.P. Zharov. In vivo flow cytometry: A horizon of opportunities. *Cytometry*. **79A**, 737-745 (2011).

19. E.I. Galanzha, M. Sarimollaoglu, D.A. Nedosekin, S.G. Keyrouz, J.L. Mehta, V.P. Zharov. In vivo flow cytometry of circulating clots using negative photototothermal and photoacoustic contrasts. *Cytometry*. **79A**, 814-824 (2011).

20. E.I. Galanzha, V.P. Zharov. In vivo photoacoustic and phototohermal cytometry for monitoring multiple blood rheology parameters. *Cytometry*. **79A**, 746-757 (2011).

21. M. Proskurnin, E.I. Galanzha, D.M. Mock, V.P. Zharov. In vivo multispectral photoacoustic and photothermal flow cytometry with multicolor dyes: A potential for real-time assessment of circulation, dye-cell interaction, and blood volume. *Cytometry.* **79A***,* 834-847 (2011).

Appendix A: Files of peer-reviewed papers are attached to the report.

Apendix B: Abstracts of Journal Articles (totally or partially supported by this program).

ACS Nano. 2011 Sep 27;5(9):7020-33. doi: 10.1021/nn2016259. Epub 2011 Sep 7

Zhang Y, Xu Y, Li Z, Chen T, Lantz SM, Howard PC, Paule MG, Slikker W Jr, Watanabe F, Mustafa T, Biris AS, Ali SF.

Mechanistic toxicity evaluation of uncoated and PEGylated single-walled carbon nanotubes in neuronal PC12 cells.

We investigated and compared the concentration-dependent cytotoxicity of single-walled carbon nanotubes (SWCNTs) and SWCNTs functionalized with polyethylene glycol (SWCNT-PEGs) in neuronal PC12 cells at the biochemical, cellular, and gene expressional levels. SWCNTs elicited cytotoxicity in a concentration-dependent manner, and SWCNT-PEGs exhibited less cytotoxic potency than uncoated SWCNTs. Reactive oxygen species (ROS) were generated in both a concentration- and surface coating-dependent manner after exposure to these nanomaterials, indicating different oxidative stress mechanisms. More specifically, gene expression analysis showed that the genes involved in oxidoreductases and antioxidant activity, nucleic acid or lipid metabolism, and mitochondria dysfunction were highly represented. Interestingly, alteration of the genes is also surface coating-dependent with a good correlation with the biochemical data. These findings suggest that surface functionalization of SWCNTs decreases ROS-mediated toxicological response *in vitro*.

J Appl Toxicol. 2012 May;32(5):365-75. doi: 10.1002/jat.1742. Epub 2011 Dec 6.

Karmakar A, Iancu C, Bartos DM, Mahmood MW, Ghosh A, Xu Y, Dervishi E, Collom SL, Khodakovskaya M, Mustafa T, Watanabe F, Biris AR, Zhang Y, Ali SF, Casciano D, Hassen S, Nima Z, Biris AS.

Raman spectroscopy as a detection and analysis tool for in vitro specific targeting of pancreatic cancer cells by EGF-conjugated, single-walled carbon nanotubes.

Single-walled carbon nanotubes (SWCNTs) were covalently linked to epidermal growth factor (EGF) proteins through an esterification process that was found to be responsible for the docking of SWCNTs on the human pancreatic cancer cells (PANC-1) surface, thus providing a mechanism for the enhanced delivery and internalization of the nanotubes. Micro Raman spectroscopy and enzyme-linked immunosorbent assay were used to evaluate the delivery process and kinetics of the SWCNTs. In vitro studies indicated that the delivery kinetics of SWCNT-EGF conjugates, at a concentration of 85 μg ml(-1), to the PANC-1 cell surfaces was significant in the first 30 min of incubation, but reached a plateau with time in accordance with the establishment of equilibrium between the association and the dissociation of EGF with the cell receptors. SWCNT-EGF conjugates could act as strong thermal ablation agents and could induce higher percentages of cellular death compared with the nontargeted SWCNTs alone.

J. Phys. Chem. C. 2011, *115* (39), pp 18967–18976 **DOI:** 10.1021/jp203474y Publication Date (Web): August 24, 2011

Alexandru R. Biris, Meena Mahmood, Mihaela D. Lazar, Enkeleda Dervishi, Fumiya Watanabe,Thikra Mustafa, Grigore Baciut, Mihaela Baciut, Simion Bran, Syed Ali, and Alexandru S. Biris

Novel Multicomponent and Biocompatible Nanocomposite Materials Based on Few-Layer Graphenes Synthesized on a Gold/Hydroxyapatite Catalytic System with Applications in Bone Regeneration

We present the synthesis of few-layer graphenes over a novel Au/hydroxyapatite catalytic system by radio-frequency chemical vapor deposition, with acetylene and methane as the carbon sources. The synthesis time was found to influence linearly the dimensions of the graphitic layers and asymptotically their corresponding thermal decomposition temperature. The resulting multicomponent nanocomposite material formed out of graphene layers, Au nanoparticles (AuNPs) supported on the surface of hydroxyapatite nanoparticles, was found to have good biocompatibility and induce excellent bone cellular proliferation. Such multicomponent composites could find numerous applications in the area of bone regeneration given the excellent biocompatibility, 3D structure, and unique composition.

Applied Physics Letters 07/2011; 99(1):013702-013702-3. DOI:10.1063/1.3607283

Abhijit Biswas, Timothy C. Ovaert, Constance Slaboch, He Zhao, Ilker S. Bayer, A.S. Biris, Tao Wang.

Mineral concentration dependent modulation of mechanical properties of bone-inspired bionanocomposite scaffold

We demonstrate tunable mechanical properties of bone-inspired bionanocomposite scaffolds while maintaining the required viscoelasticity. Mechanical properties such as hardness and elastic modulus of the bionanocomposite scaffolds were controlled by varying mineral concentrations of the bioscaffold. In particular, higher calcium and oxygen contents in the bioscaffold resulted in a significant enhancement in hardness and modulus of the bionanocomposite. Moreover, the phosphorous content appeared to be a determining factor in the hardness and mechanical properties of the bionanocomposites. These results open up the possibility of designing new engineered biocompatible nanoscaffolds with desired and tunable biomimetic functions and biomechanical properties with significant potential for advanced bone tissue engineering platforms and bone substitutes.

Journal of Materials Chemistry vol. 21 issue 34 August 16, 2011. p. 12761-12769. DOI: 10.1039/c1jm10569h. ISSN: 0959-9428.

Karmakar, Alokita; Xu, Yang; Mahmood, Meena W.; Zhang, Yongbin; Saeed, Lamya Mohammed; Mustafa, Thikra; Ali, Syed; Biris, Alexandru R.; Biris, Alexandru S.

Radio-frequency induced *in vitro* thermal ablation of cancer cells by EGF functionalized carbon-coated magnetic nanoparticles.

Carbon-shelled, iron-based magnetic nanoparticles (C/Fe MNPs) were found to act as strong heat generating agents when exposed to radio-frequency (RF) energy with the ability to thermally destroy cancer cells. In order to efficiently deliver MNPs to cancer cells and to enhance the effectiveness of the RF treatment, human epidermal growth factor (EGF) was bioconjugated with the C/Fe MNPs for their specific delivery to two cancer cell lines, MCF-7 breast cancer cells and Panc-1 pancreatic cancer cells, respectively. These cell lines overexpress the epidermal growth factor receptors (EGFRs) and were used in this study as models. EGF-MNPs have shown higher surface binding efficiency towards the MCF-7 cells based on the comparative ζ-potential measurements. Confocal optical microscopy further confirmed that EGF-bioconjugated MNPs highly accumulated around and inside of these cancer cells. RF treatment was found to destroy 92.8% of MCF-7 breast cancer cells during 10 minutes of treatment when EGF was bound to the nanoparticles, while 37.3% of cells died when MNPs alone were used in identical conditions. Panc-1 cancer cells exhibit a higher resistance than MCF-7 cells when they were exposed to MNPs or RF treatment. Cytotoxicity studies demonstrated that the EGF-C/Fe MNP bioconjugates present lower toxicity compared to the C/Fe MNP. Caspase assay studies demonstrated that the MCF-7 cancer cells underwent an apoptotic process by the caspase 3 deficiency pathway showing no evidence of morphological changes such as membrane blebbing.

Carbon 49 (2011) 4403-4411

Alexandru R. Biris, Stefania Ardelean, Dan Lupu, Ioan Misan, Cornel Iancu, Dana Monica Bartos, Ioana Rada Ilie, Enkeleda Dervishi, Yang Xu, Abhijit Biswas, Alexandru S. Biris

Studies on near infrared optical absorption, Raman scattering, and corresponding thermal properties of single- and double-walled carbon nanotubes for possible cancer targeting and laser-based ablation

We report the photo-thermal properties of single and double wall carbon nanotubes (CNT) dispersed in various solvents with different concentrations when exposed to near infrared nm laser irradiations. All these studies were correlated to the dispersivity of CNT in various solvents. The observed temperature increase of the various nanotube solutions was found to be determined by the concentration of the optically active nanotubes, as determined from their Raman scattering spectra, which are resonant in the spectral range of the laser excitation. Such findings could significantly improve the understanding of the optically active CNT species, their overall laser induced-heating levels, and thus reducing the amount of the CNT required for bio-medical photothermal applications to limit the possible undesired cytotoxic effects that occur at high nanotube concentrations. Our studies open up the possibility of using selective species of CNT as effective low-toxic photo thermal agents for cancer targeting and ablation.

ACS Nano. 2011 Jun 28;5(6):4490-503. doi: 10.1021/nn1035312. Epub 2011 Jun 3.

Orza A, Soritau O, Olenic L, Diudea M, Florea A, Rus Ciuca D, Mihu C, Casciano D, Biris AS.

Electrically conductive gold-coated collagen nanofibers for placental-derived mesenchymal stem cells enhanced differentiation and proliferation.

Gold-coated collagen nanofibers (GCNFs) were produced by a single-step reduction process and used for the growth and differentiation of human adult stem cells. The nanomaterials were characterized by a number of analytical techniques including electron microscopy and spectroscopy. They were found to be biocompatible and to improve the myocardial and neuronal differentiation process of the mesenchymal stem cells isolated from the placental chorionic component. The expression of specific differentiation markers (atrium, natriuretic peptide, actin F and actin monomer, glial fibrilary acidic protein, and neurofilaments) was investigated by immunocytochemistry.

J. Cell. Mol. Med. Vol 15, No 11, 2011 pp. 2297-2306

Meena Mahmood, Zhiguang Li, Daniel Casciano, Mariya V. Khodakovskaya, Tao Chen, Alokita Karmakar, Enkeleda Dervishi, Yang Xu, Thikra Mustafa, Fumiya Watanabe, Ashley Fejleh,

Morgan Whitlow, Mustafa Al-Adami, Anindya Ghosh, Alexandru S. Biris

Nanostructural materials increase mineralization in bone cells and affect gene expression through miRNA regulation

We report that several nanomaterials induced enhanced mineralization (increased numbers and larger areas of mineral nests) in MC3T3-E1 bone cells, with the highest response being induced by silver nanoparticles (AgNPs). We demonstrate that AgNPs altered microRNA expression resulting in specific gene expression associated with bone formation. We suggest that the identified essential transcriptional factors and bone morphogenetic proteins play an important role in activation of the process of mineralization in bone cells exposed to AgNPs.

Advanced Engineering Materials Special Issue: 3D-Imaging of Materials and Systems
Volume 13, Issue 3, pages B95–B101, March, 2011

Meena Mahmood, Philip Fejleh, Alokita Karmakar, Ashley Fejleh, Yang Xu, Ganesh Kannarpady, Hidetaka Ishihara, Rajesh Sharma, Zhongrui Li, Anindya Ghosh, Steve Trigwell, Franklin D. Hardcastle, Daniel Casciano, Guna Selvaduray, Alexandru S. Biris

Enhanced Bone Cells Growth and Proliferation on TiO_2 Nanotubular Substrates Treated by RF Plasma Discharge

Titanium implants are well known for their biocompatibility, especially if bioinertness is desired, due to the TiO_2 native oxide which is thermodynamically and chemically very stable. One of the major problems with this material involve its inability to induce enhanced cellular adhesion and proliferation on its surface without complicated structural approaches, leading to the possible lack of bone-implant interfacial interaction and rejection. In order to potentially improve osseointegration of such implants self-assembled vertical and ordered nanotubular TiO_2 arrays were fabricated by electrochemical anodization and were plasma treated under O_2, N_2, $O_2 + N_2$, and He gaseous environments and their properties analyzed by various analytical procedures. Osteoblast bone cells (MC3T3-E1) were grown on TiO_2nanotube-arrayed substrates and their proliferation was analyzed and quantified. Oxygen and nitrogen plasma treatments were found to significantly improve the proliferation of the bone cells over the TiO_2 nanoarray substrates, with the $O_2 + N_2$ combination yielding the most significant improvements. These findings may be explained by the interactions between the cells and the changes in the surface chemistry induced by the O_2 and N_2 groups introduced by the plasma discharge treatment onto the TiO_2 surfaces.

Int J Nanomedicine. 2011; 6: 1045–1055. Published online 2011 May 18. doi: 10.2147/IJN.S17684

Ethylenediamine Functionalized Single-Walled Nanotube (f-SWNT)-Assisted In vitro Delivery of Oncogene Suppressor p53 Gene to Breast Cancer MCF-7 Cells.

Alokita Karmakar, Stacie M Bratton, Enkeleda Dervishi, Anindya Ghosh, Meena Mahmood, Yang Xu, Lamya Mohammed Saeed, Thikra Mustafa, Dan Casciano, Anna Radominska-Pandya, and Alexandru S Biris

A gene delivery concept based on ethylenediamine-functionalized single-walled carbon nanotubes (f-SWCNTs) using the oncogene suppressor p53 gene as a model gene was

successfully tested in vitro in MCF-7 breast cancer cells. The f-SWCNTs-p53 complexes were introduced into the cell medium at a concentration of 20 μg mL^{-1} and cells were exposed for 24, 48, and 72 hours. Standard ethidium bromide and acridine orange assays were used to detect apoptotic cells and indicated that a significantly larger percentage of the cells (approx 40%) were dead after 72 hours of exposure to f-SWCNTs-p53 as compared to the control cells, which were exposed to only p53 or f-SWCNTs, respectively. To further support the uptake and expression of the genes within the cells, green fluorescent protein-tagged p53, attached to the f-SWCNTs was added to the medium and the complex was observed to be strongly expressed in the cells. Moreover, caspase 3 activity was found to be highly enhanced in cells incubated with the f-SWCNTs-p53 complex, indicating strongly induced apoptosis. This system could be the foundation for novel gene delivery platforms based on the unique structural and morphological properties of multi-functional nanomaterials.

ACS Nano. 2010 Jun 22;4(6):3181-6. doi: 10.1021/nn1007176.

Zhang Y, Ali SF, Dervishi E, Xu Y, Li Z, Casciano D, Biris AS.

Cytotoxicity effects of graphene and single-wall carbon nanotubes in neural phaeochromocytoma-derived PC12 cells.

Graphitic nanomaterials such as graphene layers (G) and single-wall carbon nanotubes (SWCNT) are potential candidates in a large number of biomedical applications. However, little is known about the effects of these nanomaterials on biological systems. Here we show that the shape of these materials is directly related to their induced cellular toxicity. Both G and SWCNT induce cytotoxic effects, and these effects are concentration- and shape-dependent. Interestingly, at low concentrations, G induced stronger metabolic activity than SWCNT, a trend that reversed at higher concentrations. Lactate dehydrogenase levels were found to be significantly higher for SWCNT as compared to the G samples. Moreover, reactive oxygen species were generated in a concentration- and time-dependent manner after exposure to G, indicating an oxidative stress mechanism. Furthermore, time-dependent caspase 3 activation after exposure to G (10 microg/mL) shows evidence of apoptosis. Altogether these studies suggest different biological activities of the graphitic nanomaterials, with the shape playing a primary role.

Contrast Media Mol Imaging. 2011 Sep-Oct;6(5):346-69. doi: 10.1002/cmmi.455.

de la Zerda A, Kim JW, Galanzha EI, Gambhir SS, Zharov VP.

Advanced contrast nanoagents for photoacoustic molecular imaging, cytometry, blood test and photothermal theranostics.

Various nanoparticles have raised significant interest over the past decades for their unique physical and optical properties and biological utilities. Here we summarize the vast applications of advanced nanoparticles with a focus on carbon nanotube (CNT)-based or CNT-catalyzed contrast agents for photoacoustic (PA) imaging, cytometry and theranostics applications based on the photothermal (PT) effect. We briefly review the safety and potential toxicity of the PA/PT contrast nanoagents, while showing how the physical properties as well as multiple biological

coatings change their toxicity profiles and contrasts. We provide general guidelines needed for the validation of a new molecular imaging agent in living subjects, and exemplify these guidelines with single-walled CNTs targeted to α(v) β(3) , an integrin associated with tumor angiogenesis, and golden carbon nanotubes targeted to LYVE-1, endothelial lymphatic receptors. An extensive review of the potential applications of advanced contrast agents is provided, including imaging of static targets such as tumor angiogenesis receptors, in vivo cytometry of dynamic targets such as circulating tumor cells and nanoparticles in blood, lymph, bones and plants, methods to enhance the PA and PT effects with transient and stationary bubble conjugates, PT/PA Raman imaging and multispectral histology. Finally, theranostic applications are reviewed, including the nanophotothermolysis of individual tumor cells and bacteria with clustered nanoparticles, nanothrombolysis of blood clots, detection and purging metastasis in sentinel lymph nodes, spectral hole burning and multiplex therapy with ultrasharp rainbow nanoparticles.

Nature Photonics **5**,110–116 (2011) doi:10.1038/nphoton.2010.280

Vladimir P. Zharov

Ultrasharp nonlinear photothermal and photoacoustic resonances and holes beyond the spectral limit

High-resolution nonlinear laser spectroscopy based on absorption saturation, Lamb-dip and spectral hole-burning phenomena has contributed much to basic and applied photonics. Here, a laser spectroscopy based on nonlinear nanobubble-related photothermal and photoacoustic phenomena is presented. It shows ultrasharp resonances and dips up to a few nanometres wide in broad plasmonic spectra of nanoparticles. It also demonstrates narrowing of absorption spectra of dyes and cellular chromophores, as well as an increase in the sensitivity and resolution of the spectral hole-burning technique. This approach can permits the study of nonlinear plasmonics at a level of resolution beyond the spectral limits, the identification of weakly absorbing spectral holes, spectral optimization of photothermal nanotherapy, measurements of tiny red and blue resonance shifts in nanoplasmonic sensors, the use of negative contrast in photoacoustic technique, multispectral imaging and multicolour cytometry.

Opt Lett. 2011 Oct 15;36(20):4086-8. doi: 10.1364/OL.36.004086.

Sarimollaoglu M, Nedosekin DA, Simanovsky Y, Galanzha EI, Zharov VP.

In vivo photoacoustic time-of-flight velocity measurement of single cells and nanoparticles.

Optical techniques for in vivo measurement of blood flow velocity are not quite applicable for determination of velocity of individual cells or nanoparticles. Here, we describe a photoacoustic time-of-flight method to measure the velocity of individual absorbing objects by using single and multiple laser beams. Its capability was demonstrated in vitro on blood vessel phantom and in vivo on an animal (mouse) model for estimating velocity of gold nanorods, melanin nanoparticles, erythrocytes, leukocytes, and circulating tumor cells in the broad range of flow velocity from 0.1 mm/s to 14 cm/s. Object velocity can be used to identify single cells circulating

at different velocities or cell aggregates and to determine a cell's location in a vessel cross-section.

Cytometry A. 2011 Oct;79(10):825-33. doi: 10.1002/cyto.a.21102. Epub 2011 Jul 22.

Nedosekin DA, Sarimollaoglu M, Ye JH, Galanzha EI, Zharov VP.

In vivo ultra-fast photoacoustic flow cytometry of circulating human melanoma cells using near-infrared high-pulse rate lasers.

The circulating tumor cells (CTCs) appear to be a marker of metastasis development, especially, for highly aggressive and epidemically growing melanoma malignancy that is often metastatic at early stages. Recently, we introduced in vivo photoacoustic (PA) flow cytometry (PAFC) for label-free detection of mouse B16F10 CTCs in melanoma-bearing mice using melanin as an intrinsic marker. Here, we significantly improve the speed of PAFC by using a high-pulse repetition rate laser operating at 820 and 1064 nm wavelengths. This platform was used in preclinical studies for label-free PA detection of low-pigmented human CTCs. Demonstrated label-free PAFC detection, low level of background signals, and favorable safety standards for near-infrared irradiation suggest that a fiber laser operating at 1064 nm at pulse repetition rates up to 0.5 MHz could be a promising source for portable clinical PAFC devices. The possible applications can include early diagnosis of melanoma at the parallel progression of primary tumor and CTCs, detection of cancer recurrence, residual disease and real-time monitoring of therapy efficiency by counting CTCs before, during, and after therapeutic intervention. Herewith, we also address sensitivity of label-free detection of melanoma CTCs and introduce in vivo CTC targeting by magnetic nanoparticles conjugated with specific antibody and magnetic cells enrichment.

Cytometry A. 2011 Oct;79(10):737-45. doi: 10.1002/cyto.a.21143. Epub 2011 Sep 13.

Tuchin VV, Tárnok A, Zharov VP.

In vivo flow cytometry: a horizon of opportunities.

Flow cytometry (FCM) has been a fundamental tool of biological discovery for manyyears. Invasive extraction of cells from a living organism, however, may lead to changes in cell properties and prevents studying cells in their native environment. These problems can be overcome by use of in vivo FCM, which provides detection and imaging of circulating normal and abnormal cells directly in blood or lymph flow. The goal of this review is to provide a brief history, features, and challenges of this new generation of FCM methods and instruments. Spectrum of possibilities of in vivo FCM in biological science (e.g., cell metabolism, immune function, or apoptosis) and medical fields (e.g., cancer, infection, and cardiovascular disorder) including integrated photoacoustic-photothermal theranostics of circulating abnormal cells are discussed with focus on recent advances of this new platform.

Cytometry A. 2011 October ; 79(10): 814–824. doi:10.1002/cyto.a.21106.

Ekaterina I. Galanzha, Mustafa Sarimollaoglu, Dmitry A. Nedosekin, Salah G. Keyrouz, Jawahar L. Mehta, and Vladimir P. Zharov

***In vivo* flow cytometry of circulating clots using negative photothermal and photoacoustic contrasts**

Conventional photothermal (PT) and photoacousic (PA) imaging, spectroscopy, and cytometry are preferentially based on positive PT/PA effects, when signals are above background. Here, we introduce PT/PA technique based on detection of negative signals below background. Among various new applications, we propose label-free in vivo flow cytometry of circulating clots. No method has been developed for the early detection of clots of different compositions as a source of severe thromboembolisms including ischemia at strokes and myocardial dysfunction at heart attack. When a low-absorbing, platelet-rich clot passes a laser-irradiated vessel volume, a transient decrease in local absorption results in an ultrasharp negative PA hole in blood background. Using this phenomenon alone or in combination with positive contrasts, we demonstrated identification of white, red and mixed clots on a mouse model of myocardial infarction and human blood. The concentration and size of clots were measured with threshold down to few clots in the entire circulation with size as low as 20 μm. This multiparameter diagnostic platform using portable personal high-speed flow cytometer with negative dynamic contrast mode has potential to realtime defining risk factors for cardiovascular diseases, and for prognosis and prevention of stroke or use clot count as a marker of therapy efficacy. Possibility for label-free detection of platelets, leukocytes, tumor cells or targeting them by negative PA probes (e.g., nonabsorbing beads or bubbles) is also highlighted.

Cytometry A. 2011 Oct;79(10):834-47. doi: 10.1002/cyto.a.21127. Epub 2011 Sep 8.

Proskurnin MA, Zhidkova TV, Volkov DS, Sarimollaoglu M, Galanzha EI, Mock D, Nedosekin DA, Zharov VP.

In vivo multispectral photoacoustic and photothermal flow cytometry with multicolor dyes: a potential for real-time assessment of circulation, dye-cell interaction, and blood volume.

Recently, photoacoustic (PA) flow cytometry (PAFC) has been developed for in vivo detection of circulating tumor cells and bacteria targeted by nanoparticles. Here, we propose multispectral PAFC with multiple dyes having distinctive absorption spectra as multicolor PA contrast agents. As a first step of our proof-of-concept, we characterized high-speed PAFC capability to monitor the clearance of three dyes (Indocyanine Green [ICG], Methylene Blue [MB], and Trypan Blue [TB]) in an animal model in vivo and in real time. We observed strong dynamic PA signal fluctuations, which can be associated with interactions of dyes with circulating blood cells and plasma proteins. PAFC demonstrated enumeration of circulating red and white blood cells labeled with ICG and MB, respectively, and detection of rare dead cells uptaking TB directly in bloodstream. The possibility for accurate measurements of various dye concentrations including Crystal Violet and Brilliant Green were verified in vitro using complementary to PAFC photothermal (PT) technique and spectrophotometry under batch and flow conditions. We further analyze the potential of integrated PAFC/PT spectroscopy with multiple dyes for rapid and accurate measurements of circulating blood volume without a priori information on hemoglobin content, which is impossible with existing optical techniques. This is important in many medical conditions including surgery and trauma with extensive blood loss, rapid fluid administration, and transfusion of red blood cells. The potential for developing a robust clinical PAFC prototype that is safe for human, and its applications for studying the liver function are further highlighted.

Adv Healthc Mater. 2012 Jul;1(4):493-501. doi: 10.1002/adhm.201200079. Epub 2012 Jun 4.

Xu Y, Karmakar A, Heberlein WE, Mustafa T, Biris AR, Biris AS.

Multifunctional magnetic nanoparticles for synergistic enhancement of cancer treatment by combinatorial radio frequency thermolysis and drug delivery.

Few-layer, carbon-coated, iron (C/Fe) magnetic nanoparticles (MNPs) were synthesized with controlled sizes ranging from 7 to 9 nm. The additional loading of two anti-cancer drugs, doxorubicin and erlotinib, was achieved through stacking onto the carbon shells. Controlled release of the drugs was successfully triggered by radio frequency (RF) heating or pH variation. Based on the experimental results, C/Fe MNPs act as heat-inducing agents and are able to thermally destroy cancer cells when RF is applied. It was found that the combination of anti-cancer drugs (in particular a low dose of doxorubicin) and RF treatment demonstrates a synergistic effect in inducing cell death in pancreatic cancer cells. Our findings demonstrate that MNPs can be used as highly efficient multimodal nanocarrier agents for an integrated approach to cancer treatment involving triggered delivery of antineoplastic drugs and RF-induced thermal therapy.

J Nanomedic Nanotechnol 2011, 2:6 http://dx.doi.org/10.4172/2157-7439.1000118

Thikra Mustafa, Fumiya Watanabe, William Monroe, Meena Mahmood, Yang Xu, Lamya Mohammed Saeed, Alokita Karmakar, Dan Casciano, Syed Ali and Alexandru S. Biris

Impact of Gold Nanoparticle Concentration on their Cellular Uptake by MC3T3-E1 Mouse Osteoblastic Cells as Analyzed by Transmission Electron Microscopy

The uptake mechanisms and kinetics of gold nanoparticles (AuNPs) by mouse calvaria osteoblastic cells have been studied by transmission electron microscopy (TEM). The average size of the as-synthesized AuNPs used in this study was 12.2 (± 1.3) nm, and they were used to expose MC3T3-E1 osteoblastic cells at two concentrations (10 and 160 μg/ml) for 6, 24, and 96 hours before TEM imaging. Based on this analysis, we propose that the uptake mechanism of AuNPs is concentration-dependent. At the higher concentration (160 μg/ml), the particles seem to penetrate inside the cells primarily by endocytosis as the cells engulf AuNPs as agglomerates formed on the outer cellular membrane. At the lower concentrations of 10 μg/ml, AuNPs are more likely to cross the plasma membrane individually through diffusion. Therefore, the average diameters of the nanoparticles are expected to have a significant role only when exposed to cells in low concentrations. Moreover, cytotoxicity assays showed no toxic effects of the AuNPs when MC3T3-E1 cells were exposed to concentrations used in the experiments.

J Appl Toxicol. 2012 May;32(5):365-75. doi: 10.1002/jat.1742. Epub 2011 Dec 6.

Karmakar A, Iancu C, Bartos DM, Mahmood MW, Ghosh A, Xu Y, Dervishi E, Collom SL, Khodakovskaya M, Mustafa T, Watanabe F, Biris AR, Zhang Y, Ali SF, Casciano D, Hassen S, Nima Z, Biris AS.

Raman Spectroscopy as a Detection and Analysis Tool for In Vitro Specific Targeting of Pancreatic Cancer Cells by EGF-Conjugated Single-Walled Carbon Nanotubes

Single-walled carbon nanotubes (SWCNTs) were covalently linked to epidermal growth factor (EGF) proteins through an esterification process that was found to be responsible for the

docking of SWCNTs on the human pancreatic cancer cells (PANC-1) surface, thus providing a mechanism for the enhanced delivery and internalization of the nanotubes. Micro Raman spectroscopy and enzyme-linked immunosorbent assay were used to evaluate the delivery process and kinetics of the SWCNTs. In vitro studies indicated that the delivery kinetics of SWCNT-EGF conjugates, at a concentration of 85 μg ml(-1), to the PANC-1 cell surfaces was significant in the first 30 min of incubation, but reached a plateau with time in accordance with the establishment of equilibrium between the association and the dissociation of EGF with the cell receptors. SWCNT-EGF conjugates could act as strong thermal ablation agents and could induce higher percentages of cellular death compared with the nontargeted SWCNTs alone.

J. Mater. Chem., 2012, 22, 20128-20142 DOI: 10.1039/C2JM32792A

Yang Xu, Wolf E. Heberlein, Meena Mahmood, Anamaria Ioana Orza, Alokita Karmakar, Thikra Mustafa, Alexandru R. Biris, Daniel Casciano and Alexandru S. Biris

Progress in materials for thermal ablation of cancer cells

Owing to the complexity of cancer biology, successful treatments must make use of multidisciplinary approaches that include genetic biology, materials science, chemistry, and physics. The development of nanotechnology as a mature science has provided new tools for the early detection and treatment of cancer by combining the synthesis of multifunctional nanosystems with the advanced capability of the targeted delivery of drugs and genes down to a single cell level. Nanomaterials with their unique optical, magnetic, and electrical properties have proven to be excellent candidates as thermal agents under the excitation of various electromagnetic fields (laser, alternating magnetic fields, or radiofrequency) that are capable of producing enough thermal energy for the specific destruction of the cancer cells both *in vitro* and *in vivo*. As a result, the use of such nanomaterials could open a new field in the area of cancer medicine given their ability to act as high resolution contrast agents and to thermally ablate tumors or individual cancer cells and to overcome some of the current limitations in cancer treatment.

J Biophotonics. 2013 May;6(5):425-34. doi: 10.1002/jbio.201200047. Epub 2012 Aug 20.

Nedosekin DA, Sarimollaoglu M, Galanzha EI, Sawant R, Torchilin VP, Verkhusha VV, Ma J, Frank MH, Biris AS, Zharov VP.

Synergy of photoacoustic and fluorescence flow cytometry of circulating cells with negative and positive contrasts.

In vivo photoacoustic (PA) and fluorescence flow cytometry were previously applied separately using pulsed and continuous wave lasers respectively, and positive contrast detection mode only. This paper introduces a real-time integration of both techniques with positive and negative contrast modes using only pulsed lasers. Various applications of this new tool are summarized, including detection of liposomes loaded with Alexa-660 dye, red blood cells labeled with Indocyanine Green, B16F10 melanoma cells co-expressing melanin and green fluorescent protein (GFP), C8161-GFP melanoma cells targeted by magnetic nanoparticles, MTLn3 adenocarcinoma cells expressing novel near-infrared iRFP protein, and quantum dot-carbon nanotube conjugates. Negative contrast flow cytometry provided label-free detection of low absorbing or weakly fluorescent cells in blood absorption and autofluorescence background, respectively. The use of pulsed laser for time-resolved discrimination of objects with long

fluorescence lifetime (e.g., quantum dots) from shorter autofluorescence background (e.g., blood plasma) is also highlighted in this paper. The supplementary nature of PA and fluorescence detection increased the versatility of the integrated method for simultaneous detection of probes and cells having various absorbing and fluorescent properties, and provided verification of PA data using a more established fluorescence based technique.

Methods. 2012 Jul;57(3):280-96. doi: 10.1016/j.ymeth.2012.06.009. Epub 2012 Jun 26.

Galanzha EI, Zharov VP.

Photoacoustic flow cytometry.

Conventional flow cytometry using scattering and fluorescent detection methods has been a fundamental tool of biological discoveries for many years. Invasive extraction of cells from a living organism, however, may lead to changes in cell properties and prevents the long-term study of cells in their native environment. Here, we summarize recent advances of new generation flow cytometry for in vivo noninvasive label-free or targeted detection of cells in blood, lymph, bone, cerebral and plant vasculatures using photoacoustic (PA) detection techniques, multispectral high-pulse-repetition-rate lasers, tunable ultrasharp (up to 0.8 nm) rainbow plasmonic nanoprobes, positive and negative PA contrasts, in vivo magnetic enrichment, time-of-flight cell velocity measurement, PA spectral analysis, and integration of PA, photothermal (PT), fluorescent, and Raman methods. Unique applications of this tool are reviewed with a focus on ultrasensitive detection of normal blood cells at different functional states (e.g., apoptotic and necrotic) and rare abnormal cells including circulating tumor cells (CTCs), cancer stem cells, pathogens, clots, sickle cells as well as pharmokinetics of nanoparticles, dyes, microbubbles and drug nanocarriers. Using this tool we discovered that palpation, biopsy, or surgery can enhance CTC release from primary tumors, increasing the risk of metastasis. The novel fluctuation flow cytometry provided the opportunity for the dynamic study of blood rheology including red blood cell aggregation and clot formation in different medical conditions (e.g., blood disorders, cancer, or surgery). Theranostics, as a combination of PA diagnosis and PT nanobubble-amplified multiplex therapy, was used for eradication of CTCs, purging of infected blood, and thrombolysis of clots using PA guidance to control therapy efficiency. In vivo flow cytometry using a portable fiber-based devices can provide a breakthrough platform for early diagnosis of cancer, infection and cardiovascular disorders with a potential to inhibit, if not prevent, metastasis, sepsis, and strokes or heart attack by well-timed personalized therapy.

Sci Rep. 2013;3:1293. doi: 10.1038/srep01293.

Shao J, Griffin RJ, Galanzha EI, Kim JW, Koonce N, Webber J, Mustafa T, Biris AS, Nedosekin DA, Zharov VP.

Photothermal nanodrugs: potential of TNF-gold nanospheres for cancer theranostics.

Nanotechnology has been extensively explored for drug delivery. Here, we introduce the concept of a nanodrug based on synergy of photothermally-activated physical and biological effects in nanoparticle-drug conjugates. To prove this concept, we utilized tumor necrosis factor-alpha coated gold nanospheres (Au-TNF) heated by laser pulses. To enhance photothermal efficiency in near-infrared window of tissue transparency we explored slightly ellipsoidal nanoparticles, its clustering, and laser-induced nonlinear dynamic phenomena leading to

amplification and spectral sharpening of photothermal and photoacoustic resonances red-shifted relatively to linear plasmonic resonances. Using a murine carcinoma model, we demonstrated higher therapy efficacy of Au-TNF conjugates compared to laser and Au-TNF alone or laser with TNF-free gold nanospheres. The photothermal activation of low toxicity Au-TNF conjugates, which are in phase II trials in humans, with a laser approved for medical applications opens new avenues in the development of clinically relevant nanodrugs with synergistic antitumor theranostic action.

J Biophotonics. 2013 May;6(5):425-34. doi: 10.1002/jbio.201200047. Epub 2012 Aug 20.

Nedosekin DA, Sarimollaoglu M, Galanzha EI, Sawant R, Torchilin VP, Verkhusha VV, Ma J, Frank MH, Biris AS, Zharov VP.

Synergy of photoacoustic and fluorescence flow cytometry of circulating cells with negative and positive contrasts.

In vivo photoacoustic (PA) and fluorescence flow cytometry were previously applied separately using pulsed and continuous wave lasers respectively, and positive contrast detection mode only. This paper introduces a real-time integration of both techniques with positive and negative contrast modes using only pulsed lasers. Various applications of this new tool are summarized, including detection of liposomes loaded with Alexa-660 dye, red blood cells labeled with Indocyanine Green, B16F10 melanoma cells co-expressing melanin and green fluorescent protein (GFP), C8161-GFP melanoma cells targeted by magnetic nanoparticles, MTLn3 adenocarcinoma cells expressing novel near-infrared iRFP protein, and quantum dot-carbon nanotube conjugates. Negative contrast flow cytometry provided label-free detection of low absorbing or weakly fluorescent cells in blood absorption and autofluorescence background, respectively. The use of pulsed laser for time-resolved discrimination of objects with long fluorescence lifetime (e.g., quantum dots) from shorter autofluorescence background (e.g., blood plasma) is also highlighted in this paper. The supplementary nature of PA and fluorescence detection increased the versatility of the integrated method for simultaneous detection of probes and cells having various absorbing and fluorescent properties, and provided verification of PA data using a more established fluorescence based technique.

Head Neck. 2013 Aug 3. doi: 10.1002/hed.23439. [Epub ahead of print]

Juratli MA, Sarimollaoglu M, Siegel ER, Nedosekin DA, Galanzha EI, Suen JY, Zharov VP.

Real-time monitoring of circulating tumor cell release during tumor manipulation using in vivo photoacoustic and fluorescent flow cytometry.

BACKGROUND: Circulating tumor cells (CTCs) form metastases in distant organs. The purpose of this research was to determine if tumor manipulation could enhance cancer cell release from the primary tumor into the circulatory system.
METHODS: Nude mice were inoculated with melanoma or breast cancer cells. The implanted tumor underwent compression, biopsy, complete resection, or laser treatment. CTCs were monitored in the bloodstream using in vivo photoacoustic and fluorescence flow cytometry.
RESULTS: We discovered that pressure, biopsy, and laser treatment can dramatically increase CTC counts (up to 60-fold), whereas proper tumor resection significantly decreases CTC counts.
CONCLUSION: Standard medical procedures could trigger CTC release that may increase the risk of metastases. This finding suggests the guidance of cancer treatment and likely diagnosis

by real-time monitoring of CTC dynamics followed by well-timed treatment to reduce CTCs in the blood. In vivo detection of intervention-amplified CTCs could be used for early diagnosis of a small tumor, which is undetectable with conventional methods.